ENERGY, ENVIRONMENT & STORAGE

AN INTERNATIONAL JOURNAL

Volume-4
Issue-1
January, 2024
ISSN: 2791-6197

Editor in Chief
Dr. Selahaddin Orhan AKANSU

ENERGY, ENVIRONMENT AND STORAGE

EES JOURNAL

Founded and Published by Erciyes Energy Association

Energy, Environment and Storage Journal is indexed in Crossref

Copyright ©

Printed in Turkey

ISSN-2791-6197

EES- EDITORIAL BOARD

BOARD MEMBER

VOLUME 4, ISSUE 1, REVIEWER BOARD

EDITORIAL OFFICE

AIM AND SCOPE

Energy, Environment and Storage papers consider the prospects of energy technologies, environment, materials, process control and industrial systems. The Energy, Environment and Storage will be published 3 times per year.

Contributions describe novel and significant applications to the fields of:

- Hydrogen Fuels
- Hydrogen and Fuel Cell
- Hydrogen Economic
- Biomass
- Solar PV Technology
- Solar Thermal Applications
- Wind Energy
- Materials for Energy
- Drones and Energy Applications
- Nuclear Energy and Applications
- Hydro Power
- Fuel Technologies (CNG, LNG, LPG, Diesel, Gasoline, Ethanol, etc.)
- Numerical Modelling
- Energy Storage and Systems
- Battery Technologies
- Energy Management
- Heat and Mass Transfer
- Aerodynamics
- Aerospace and Energy Applications
- Combustion
- Electric Vehicle Transportation
- Off-grid Energy Systems
- Environment Management
- Air Pollution
- Water and Wastewater Pollution
- Water and Wastewater Management
- Waste Management
- Global Warming and Climate Change
- Environmental Ecosystem
- Environmental System Modelling and Optimization
- Ecological Applications or Conservation

VOLUME 4, ISSUE 1

JANUARY 2024

CONTENTS

Energy, Environment and Storage

Journal Homepage: www.enenstrg.com

1.4-Dioxane and the Phenolic Compound Against UV Irradiation of Diesel

Salatin Guliyeva[1], Ibrahim Mamedov[1*]

[1]*Baku State University, Baku, Azerbaijan, ORCID: 0000-0003-2412-4596 and ORCID: 0000-0002-5757-9899*

ABSTRACT. During storage and transportation, some classes of hydrocarbons in diesel fuel can undergo chemical transformations over time due to ambient temperature, sunlight, and oxygen in the air. As a result of these reactions, there are changes in the composition of the fuel, such as sediment, color change, turbidity, which have a negative effect on the physico-chemical indicators of the fuel. Such a change can cause engine wear and adversely affect engine efficiency, performance, emissions and durability. The main objective of this study is to investigate antioxidant additives to delay the aging process in diesel fuels. The compounds 1,4 dioxane and 3-hydroxy-1-(2-hydroxyphenyl)-3-(4-nitrophenyl)-propan-1-one were selected for this study. UV rays have been used to stimulate the aging process. As a result of research, the use of 1,4-dioxane has significantly improved the chemical stability, density and kinematic viscosity of fuel and its use in diesel fuel has shown greater stabilization potential.

Keywords: diesel, 1,4-dioxane, UV irradiation, chemical stability

Article History: Received: 30.09.2023; Accepted: 10.01.2024

Doi: https://doi.org/10.52924/ATMW9062

1. INTRODUCTION

As we know, diesel fuel is a complex mixture obtained from the fractional separation of crude petroleum and consists of a mixture of aliphatic, aromatic, naphthenic hydrocarbons and a small amount of heteroatomic compounds [1]. It is generally recognized that aromatic, heteroatomic and unsaturated compounds from the petroleum refinery processes present in fuels strongly influence fuel stability [2]. During storage and transportation, these types of hydrocarbons in diesel fuel can undergo chemical transformations over time due to ambient temperature, sunlight, and oxygen in the air [3-5]. In particular, the presence of polyaromatic hydrocarbons (PAHs) in petroleum diesel can accelerate fuel aging, depending on storage and transportation conditions. PAHs can be oxidized by environmental exposure. For example, some PAHs, such as perylene and benzo[a]pyrene, undergo photodegradation after solar or UV irradiation. The chemical reactions may occur inside the sample and in contact with the surroundings, notably tank walls and the atmosphere, at specific conditions. These chemical changes significantly influence the properties and exploitation indicators of the fuel, causing some problems with the stable regime and operation of diesel motors. As metal tanks are now replaced by polymer tanks with visible transparency, the photostability of the fuel becomes important [1, 6].

Adding additives such as oxidation inhibitors to diesel fuel increases its chemical stability [7]. Taking account of the above, the goal of this work is to investigate the changes in the chemical content of diesel fuel due to the influence of sunlight during storage and transportation, their effect on operational characteristics, and to find additives to prevent fuel aging. For this purpose, 1,4-dioxane and 3-hydroxy-1-(2-hydroxyphenyl)-3-(4-nitrophenyl)-propan-1-one were used as antioxidants. A lamp with a wavelength of 300–450 nm was used to stimulate natural solar irradiation. Testing of chemical changes under UV irradiation was studied using NMR spectroscopy.

2. EXPERIMENTAL

2.1 Materials and methods

Diesel fuel samples were taken from a petrol station in Baku, Azerbaijan.

To stimulate natural solar irradiation, a visible and UV-emitting PRK2-lV-59 model using a lamp with a wavelength of 300–450 nm was used.

NMR spectra were obtained on a Bruker FT NMR (UltraShieldTM Magnet) AVANCE 300 (300.130 MHz for ^{1}H and 75.468 MHz for ^{13}C) with a 5 mm sample tube using Bruker Standard software (TopSpin 3.1). The ^{1}H and ^{13}C chemical shifts were referenced to internal tetramethyl silane (TMS). NMR-grade CDCl3 was taken for the analysis of fuel samples.

2.2 Preparation of samples and UV irradiation

Three heat-resistant closed glass ampoules are taken for sample preparation. 20 ml of crude diesel (D1) for the first sample, 20 ml of diesel and 2 ml of dioxane (DD1) for the second sample and 20 ml of diesel, 2 ml of dioxane and

*Corresponding author: bsu.nmrlab@gmail.com

0.01 g of 3-hydroxy-1-(2-hydroxy-phenyl)-3-(4-nitrophenyl) propan-1-one (DDC1) for the last sample were added into appropriate glass ampoules and stirred at room temperature. The samples were irradiated for 24 hours at room temperature (20°C) using a PRK2-lV-59 model lamp emitting visible and UV (300–450 nm) light rays. Within 24 hours, visible changes occurred in each of the samples (Figure 1).

1,4-dioxane

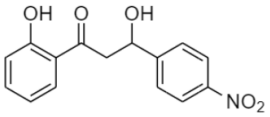

3-hydroxy-1-(2-hydroxyphenyl)-3-(4-nitrophenyl)propan-1-one

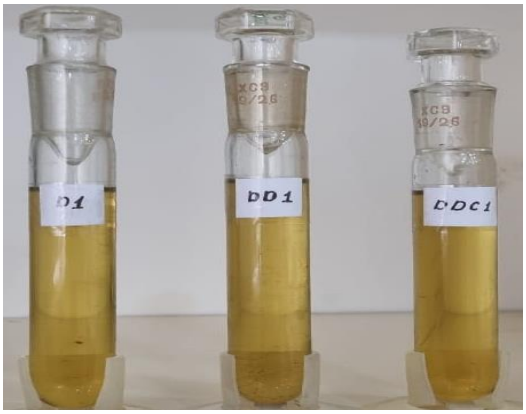

(**a**)

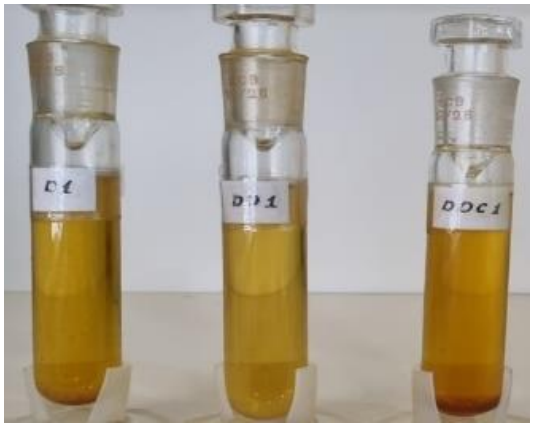

(**b**)

Figure 1. Diesel (D1), DD1, DDC1 blends before (*a*) and after (*b*) the UV irradiation

3. RESULTS AND DISCUSSION

In our previous works, information was given about the occurrence of photodegradation processes under the influence of ultraviolet irradiation, which affect the physico-chemical and exploitation properties of fuel [3]. This work is devoted to testing different performance characteristics of diesel fuel with (or without) antioxidant additives before and after exposure to ultraviolet and visible rays from the sun. D1, DD1, DDC1 fuel samples were irradiated with UV rays for 24 hours in order to study the effect of sunlight on the chemical stability of diesel fuel produced at the Heydar Aliyev Oil Refinery and to find anti-aging additives. Changes in the chemical composition of the fuel samples after the end of the storage period were studied with the help of NMR spectroscopy. The obtained results are given in Table 1.

Table 1. Hydrocarbon content of fuel blends from the ^{1}H NMR spectra before and after UV irradiation

Before UV	Par. h/c	Ole. h/c	Ar. h/c	After UV	Par. h/c	Ole. h/c	Ar. h/c
D1	95.14	0.05	4.72	**D1**	96.40	0.02	3.60
DD1	96.49	0.06	3.39	**DD1**	96.44	0.02	3.54
DDC1	96.57	0.07	3.34	**DDC1**	96.34	0.06	3.6

As can be seen from Table 1, the change in paraffinic/aromatic hydrocarbon ratio after 24 hours of UV irradiation in fuel samples D1, DD1, DDC1 was 26.8, 27.2 and 26.7%, respectively (the same results before UV irradiation were 20.2, 28.5 and 28.9). Simple diesel fuel without additives had the greatest change in chemical composition, while the diesel sample with dioxane and 3-hydroxy-1-(2-hydroxy-phenyl)-3-(4-nitrophenyl)propan-1-one additions had the least change.

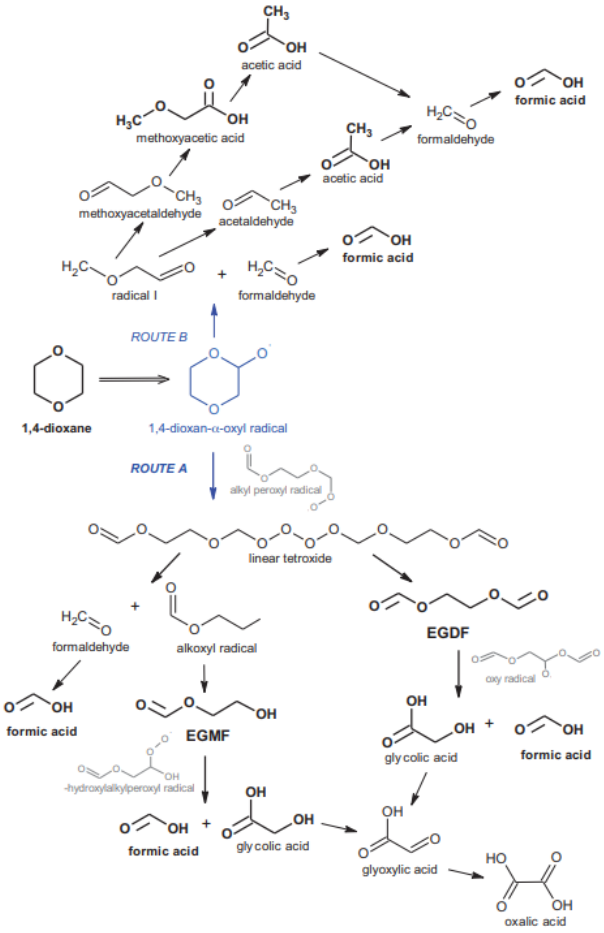

Figure 2. Simplified schematic of the major reaction pathways proposed for 1,4-dioxane degradation

Our previous work confirmed the high antioxidation property of 1,4 dioxane in fuel mixtures under high temperature conditions [8]. As a continuation of the work, the protective effects of this antioxidant additive against ultraviolet irradiation were investigated. For this purpose, a model fuel was prepared from 1,4-dioxane and hexadecane (HD) and subjected to UV irradiation for 24 hours and chemical composition changes were investigated with the help of NMR spectroscopy. However, while 1,4-dioxane itself was converted to 44% in sample DD1 and 42% in sample DDC1, no

photodegradation was observed in the reference sample HD. Due to its special chemical structure, 1,4-dioxane is not directly affected by photolysis. It is believed that the pH conditions of diesel fuel affect the photodegradation of dioxane. Thus, the photochemical decomposition of 1,4-dioxane increases in acidic fuel conditions to defend fuel from oxidation. At this time, several intermediate products, namely aldehydes, organic acids, mono- and di-formate esters of 1,2-ethanediol, are formed. Depending on the formation and re-degradation of intermediate products, pH values, irradiation time, dose, etc. have an effect (Figure 2) [9, 10]. When 1,4-dioxane added to fuel is exposed to ultraviolet rays, acid intermediates are formed from the pH change. Thus, the diesel we studied was a weakly acidic environment with a pH value of 5.8–6 [11-14]. This allows the decomposition of 1,4 dioxane into acids and aldehydes, which can be clearly seen during NMR analysis. As can be seen from Table 1, a slight decrease in paraffinic hydrocarbons and an increase in aromatic hydrocarbons region are observed in the DD1 fuel sample during photodegradation. This can be explained by the formation of acids and aldehydes from the 44% conversion of dioxane, as a result of which the peaks in the NMR ^{1}H spectrum shift to the range of aromatic hydrocarbons, which may present aldehyde, phenolic and acid hydroxyl fragments.

As we know, compounds with a long-conjugated structure consisting of aromatic rings and side chains with double bonds and carbonyl groups have UV-absorbing properties [4, 5, 15]. For this purpose, we tested the property of the phenolic compound [3-hydroxy-1-(2-hydroxyphenyl)-3-(4-nitrophenyl) propan-1-one] added to diesel fuel as a UV absorber. As can be seen from the NMR results, the addition of the compound has a positive effect on the chemical stability of the fuel. However, visually, after 24 hours of irradiation, turbidity, precipitate and discoloration were observed in the fuel sample. This can be explained by the possibility that 3-hydroxy-1-(2-hydroxyphenyl)-3-(4-nitrophenyl) propane-1-one itself decomposes into another phenolic compounds, which needs more deep investigation.

Table 2. Properties of D1, DD1, DDC1 samples before and after

Properties	ASTM Methods	ASTM Diesel
Relative density at 20°C, g/cm^3	D1298	0.82-0.86
Sulfur, ppm, max.	D 975-14	15
Viscosity at 40°C, mm^2/s	D445	1.3 - 4.1
Cetane number, min.	D613	40.00
Flash point, °C, min	D93	52

Before UV irradiation			After UV irradiation		
D1	DD1	DDC1	D1	DD1	DDC1
0,845	0,864	0,863	0,848	0,854	0,856
47	39	38	-	-	-
3,128	2,11	2,15	3,017	2,49	2,57
43,35	40,29	43,76	43,45	40,13	43,63
77	54	56	87	58	61

In the continuation of the research, the operating characteristics of petroleum diesel (D1), DD1 and DDC1 fuel mixtures were studied (Table 2). Despite the slight decrease in viscosity, ignition temperature, density, cetane number, etc. after UV irradiation, the studied fuel mixtures DD1 and DDC1 have properties that correspond to the diesel fuel standard, and the proposed mixtures can be used in diesel engines without any changes [16].

4. CONCLUSIONS

This article reports on testing the chemical stability of diesel fuel against UV radiation for 24 hours and searching for additives to ensure chemical stability. As can be seen from the obtained data, photodegradation with UV has a negative effect on the chemical stability of the fuel (change in paraffinic/aromatic hydrocarbon ratio by 32.7%) and operational properties.

One of the most important contributions of this work was to obtain a more physiochemically stable fuel mixture under the studied conditions. For this purpose, the DD1 fuel sample made on the basis of 1,4 dioxane and diesel was studied as the least sensitive to structural changes under the influence of UV rays. DD1 causes only a 4.6% change in its chemical composition after UV irradiation and retains its properties more than D1, DDC1. The DDC1 also has chemical stability under the specified conditions (structural changes: 7.6%). However, although the 3-hydroxy-1-(2-hydroxyphenyl)-3-(4-nitrophenyl) propan-1-one compound used as an additive maintained the chemical stability of the fuel sample against UV rays, it itself photodegraded after irradiation and formed a gum-like deposit on the walls of the container. At the same time, it was checked that the operating properties of the investigated fuel mixtures before and after UV irradiation were in accordance with ASTM standards.

The reported work may be interesting when studying the application of diesel fuel under different storage and transportation conditions.

Conflicts of interest

The authors declare that there are no conflicts of interest

Acknowledgments

The authors express their gratitude to the department of Petroleum chemistry and chemical technology and the Laboratory of Nuclear Magnetic Resonance at Baku State University for their support and assistance in conducting the research.

References

[1] Gad, S.C. Diesel Fuel, *Encyc. of Toxic.*, 1, 115–118, 2014.

[2] Andrea, P., Claudia, D., Elke Z. UV irradiation of natural organic matter (NOM): impact on organic carbon and bacteria, *Aqua. Scien.*, 74(3), 443–454, 2012.

[3] Guliyeva, S., Mamedov, I.G. UV irradiation testing of biodiesel from the Alhagi oil and diesel/biodiesel mixtures, *Proc. Univer. Appl. Chem.Biotech*., 3, 455-461, 2022.

[4] Dąbrowska, D., Kot-Wasik, A., Namieśnik, J. Stability studies of selected polycyclic aromatic hydrocarbons in different organic solvents and identification of their transformation products, *Polish J. of Environ. Stud*., 17(1), 17-24, 2008.

[5] Bernstein, M.P., Sandford, S.A., Allamandola, L.J., Gillette, J.S., Clemett, S.J., Zare, R.N. UV irradiation of polycyclic aromatic hydrocarbons in ices: production of alcohols, quinones, and ethers, *Science*, 283, 1135-1138, 1999.

[6] Borecki, M., Geca, M., Korwin-Pawlowski, M. Automotive diesel fuel internal stability testing with the use of UV and temperature as degradation factors, *Materials*, 15, 8548, 2022.

[7] Karavalakis, G., Stournas, S. Impact of antioxidant additives on the oxidation stability of diesel/biodiesel blends, *Ener. Fuels*, 24, 3682–3686, 2010.

[8] Mamedov, I., Mamedova, G., Azimova, N. Testing of ethylene glycol ketal, dioxane and cyclopenta none as components of B10, B20 fuel blends, *Ener. Environ. and Stor.*, 2(3), 9-12, 2022.

[9] H. Barndok, D., Hermosilla, C., Han, D.D., Dionysiou, C., Negro, A. B. Degradation of 1,4-dioxane from industrial wastewater by solar photocatalysis using immobilized NF-TiO2 composite with monodisperse TiO_2 nanoparticles, *Appl. Catal. B Environ*., 180, 44–52, 2016.

[10] Tawfik, A. Degradation pathways of 1,4-dioxane in biological and advanced oxidation processes, *Desal. and Wat. Treat.*, 178, 360-386, 2020.

[11] Xu, X., Liu, S., Smith, K., Wang, Y., Hu, H. Light-driven breakdown of 1,4-dioxane for potable reuse: A review, *Chem. Eng. J*., 373, 508-518, 2019.

[12] Vescovi, T., Coleman, H. M., Amal, R. The effect of pH on UV-based advanced oxidation technologies-1,4-Dioxane degradation, *J. Hazard Mater*., 182, 75-79, 2010.

[13] Barndõk, H., Cortijo, L., Hermosilla, D. Removal of 1,4-dioxane from industrial wastewaters: routes of decompo-sition under diff erent operational conditions to determinethe ozone oxidation capacity, *J. Hazard. Mat*., 280, 340–347, 2014.

[14] Ellappan, S., Rajendran, S. Effect of 1, 4-dioxane addition on operating characteristics of a neat biodiesels-fueled diesel engine. *Energy Sources, Part A: Recovery, Utiliz. and Environ. Effec.*, 1-14, 2019,

[15] Lin, M., Yang, L., Zhan, H., Xia, Y., He, Y., Lan, W., Ren, J., Yue, F., Lu, F. Revealing the structure-activity relationship between lignin and anti-UV radiation, *Ind. Crops Prod*. 174, 114212, 2021.

[16] Sayyed, S. Characterization of biodiesel: A Review, *Intern. J. of Engin. Res. and Techn.*, 02, 2077-2082, 2013.

Research Article

Energy, Environment and Storage (2024) 04-01:5-12

Energy, Environment and Storage

Journal Homepage: www.enenstrg.com

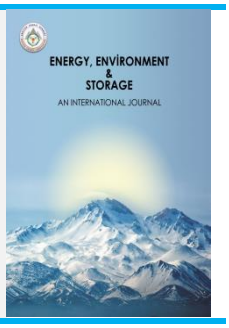

Vertical Axis Turbine Performance at Different Parameters: Effects of Generated Turbulence

Suleyman Osmanli[1,2*], S. Orhan Akansu[1], Y. Erkan Akansu[3]

[1]Erciyes University, Faculty of Engineering, Dept. of Mech. Eng. 38280, Kayseri, Turkey ORCID: 0000-0002-0085-7915
[2,]Van Yuzuncu Yil University, Faculty of Engineering, Dept of Mech. Eng., 65080, Van, Turkey ORCID: 0000-0001-8854-0332*
[3]Nigde Omer Halisdemir University, Faculty of Engineering, Dept of Mech. Eng., 51240, Nigde, Turkey ORCID: 0000-0003-0691-3225

ABSTRACT. The need to increase the energy efficiency and energy harvesting of vertical axis wind turbines is growing as a consequence of the quick expansion in the energy sector. Therefore, it is crucial to comprehend how a turbine operates. In this study, the more often used VAWT—vertical axis wind turbine—has been experimentally evaluated. Various performance graphs have been produced as a result. At various wind speeds, S1014 and S1020 airfoils are employed. Aspect ratio and angle of attack were noted, and the performance of the turbine was investigated in relation to the impact of the current produced by the turbulence generating plate. The subsonic wind tunnel setup utilized during the testing consisted of a 15 W DC motor and a 0.1 Nm torque meter. The findings demonstrated that the S1014 type blade profile was more efficient and boosted performance of the two types.

Keywords: VAWT, Turbulence, Efficiency, Sustainability, Energy.

Article History: Received: 22.07.2023; Accepted: 23.01.2024

Doi: https://doi.org/10.52924/VURM7594

1. INTRODUCTION

One of the most important issues of the current era, perhaps the most important is solving energy problems. It is gradually shifting towards sustainable energy due to energy diversity, reduction of fossil fuels, extraction costs and emission values to the environment. Therefore, there is a need for technologies that can obtain energy from nature that do not pollute the environment. Among these resources, wind power is developing rapidly and its usage area is increasing. Even in the future, the decrease in the production cost of the turbines per unit rather than the efficiency will be decisive for the use of this energy source.

The applications of small-scale wind turbines for electricity generation in rural areas are increasing. Naturally, both academic studies and commercial productions in this field are still increasing rapidly [1]. In general, wind types are divided into two as horizontal and vertical.

Although horizontal axis turbines are based on the principle of lift, they require relatively higher wind speeds. Vertical Axis Wind turbines, VAWTs are used for low-speed and low-noise areas for non-urban living spaces [2,3]. On the other hand, these systems can be installed to building in city center or special structures [4]. In some cases, researchers can place turbines in different locations. Krishnan and Paraschivoiu [11] used to obtain performance characteristics of rooftop vawt. They showed that the design of diffuse-shaped shroud provides high coefficient of performance. This type of turbines not only require lift but also works with drag force. VAWTs can be analyzed in three parts as Savonius, Darrieus and Helical [5,6]. It has been observed to be very effective in self-starting the Savonius-type turbine [7] and produces their torque at low angles of attack [8]. Darrieus was found as VAWT in the 1920s by F. M. Darrieus based on the principle of airplane aerodynamics. This principle includes different profile shape between upper and lower surface of the blade which caused lifting force by pressure difference [9]. VAWTs are unfortunately quite unsuccessful in self-starting. In order to overcome this, some studies that are used in combination with darrieus turbines are available [10]. In addition, because of the disadvantages of Darrieus VAWT over high performance and traditional horizontal axis wind turbines, the VAWT workspace is limited to unstable wind environments and analysis systems are complex [1].

Many studies have focused on increasing the VAWT's performance. [17-22]. These upgrades may primarily be divided into three groups: optimizing [23–25], adding a device [26–28], and utilizing aerodynamic interaction [29–33]. Experimental investigations have looked at performance factors in other research [12–16]. Their experimentation with several blade types suggests creating a hybrid turbine.

*Corresponding author: steksin@erciyes.edu.tr

The conflicting results of the recently published and previous research indicate that the VAWT rotor blade aerodynamics and kinematics are still not fully understood under changing wind conditions.

In this study, our aim observes the effect of turbulence on Vertical Axis Wind Turbine, VAWT and performance characteristics with two different blade profile. Many parameters were altered such as Angle of Attack, AoA, Aspect ratio, H/D, free stream velocity, $U_∞$. Comparisons were made with bare case and turbulent flow regime. Graphics are generated in TSR versus coefficient performance, Cp. Also, solidity effect was investigated. The experimental strategy is defined in Section 2, the results shown in Sections 3. In the last part, a short and concise summary of the whole study is given.

2. MATERIALS AND METHODS

This portion of the article goes into depth about the tools used in the wind tunnel and all the methods utilized to test and record VAWT performance. In this study, power output and other characteristics were examined with turbine blades. All experiments were done both in the Erciyes University, faculty of aeronautics and astronautics, subsonic wind tunnel and Nigde Omer Halisdemir University, Mechanical Engineering department aerodynamic flow control laboratory. Wind tunnel cross section has 570 x 570 mm dimensions at the entrance to test region and expands with 30 to kept constant the static pressure along the 1800 mm. 15 kW fan can reach 33 mm/s wind speed at the empty status. This subsonic wind turbine setup can be seen in figure 1.

Two different blade profiles *(S1014, S1020)* were used during the experiment. The span length, diameter of turbine, angle of attack, flow regime was altered in order to obtain power output by changing the electronically load. Rigol DL3021 brand device was used for this loading as shown in figure 2. Burster torqumeter was connected between turbine shaft and 15W Maxon DC motor.

Fig. 1. General view of the test facility.

8 channel Oros datalogger was used to collect data 1000 sampling frequency. Free stream wind velocity, $U_∞$, was measured at each case to minimize error due to the existence of turbine in the test section. Because, any obstacle in the test section can be caused 20% reduction on the free stream flow velocity.

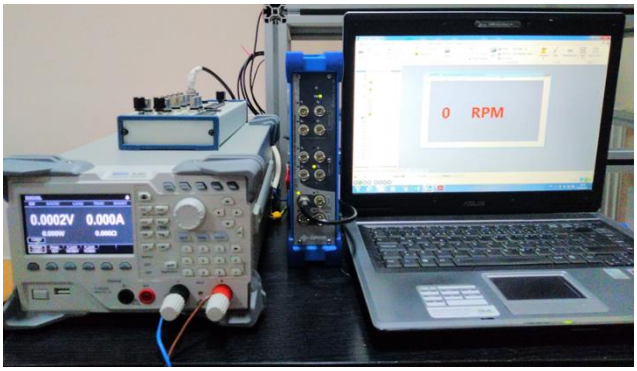

Fig. 2. Electronical load and data logger used during the experiment.

2.1 Turbine

The VAWT which is investigated consist of three bladed rotors as demonstrated in figure 3. Side view of the turbine demonstrated at a and top view of it is at b. Turbine shaft is fixed by bearing from the lower and upper parts of the test area. The height of the blades, H and diameter of turbine, D varies between 270-360 mm and 180-270 mm respectively. As a result, aspect ratio, H/D=1, 1.5 and 2 values are obtained. The blade chord has been adjusted to 60 mm and has not been changed in all turbine structures. Aluminum struts of 3 mm thickness and 15 mm width were used to connect the blades to the shaft. All metal parts were constructed with laser cutting when blades produced in 3D printer with PLA filaments.

Although different miles were used for turbine, most of them caused uncertainty during rotation. However, carbon shaft that is best choice minimizes vibration, especially at high rotation speeds, resulting in more reliable results. The air entering the test zone rotates the turbine counterclockwise. As is known, this is about the positioning of the blades.

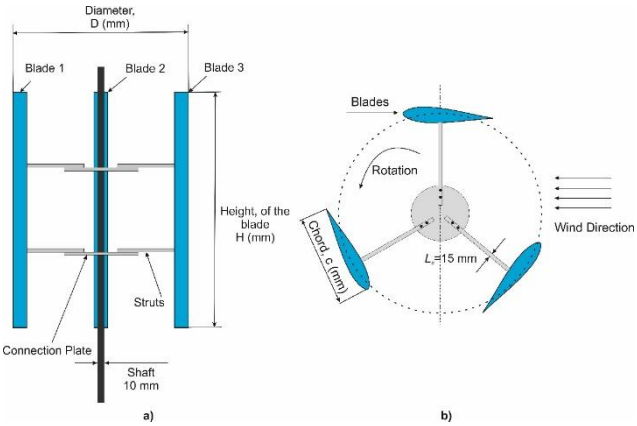

Fig. 3. Side view of the turbine a) and top view of the turbine b).

Figure 4 shows the details of connection struts and turbine blades. It has 120 mm diameters and 10 mm inner hole. There are four holes with a diameter of 3 mm each to screw the struts and plate together. Holes are specified from a to z with an angle of 5 degrees between them provided that only a-b is aligned. At each hole change, the blades have an angle of attack of 5 degrees. This produced part makes it very easy to give the turbine blades the angle of attack. At the same time, it minimizes the margin of error that may

occur when angling the blades. Moreover, the figure 4 presents the profiles of the blades used in the experiment.

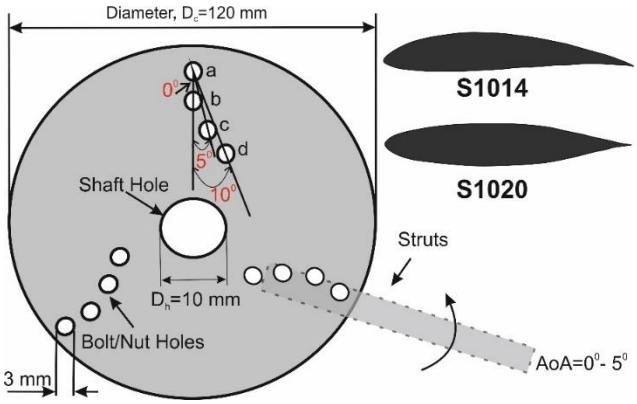

Fig. 4. Details of the connection plate and profile of blades.

A typical VAWT operates at low Tip Speed Ratios, TSR. For this reason, the wind speed has been tried to be kept in the closest possible range. In current experiment, the incoming flow speed was adjusted in the range of 4-9 m/s, and the inlet turbulence intensity is less than 1% normally when there is no vortex generator. The turbulence grid made from the metal material is located 350 mm from the front of the turbine. The main criterion for the grating's effect on flow is the porosity, β. This value can be calculated in equation 1 as given below. The porosity ratio was calculated according to equation 1 and it has 52%. Figure 5 represents the schematic view of the test set-up. The wind flow passes through the grid and reaches the turbine at a certain distance. d, expressing the turbulator diameter, was determined as 25 mm.

$$\boldsymbol{\beta = \frac{3a}{3a+b}} \qquad (1)$$

2.2 Test Facilities

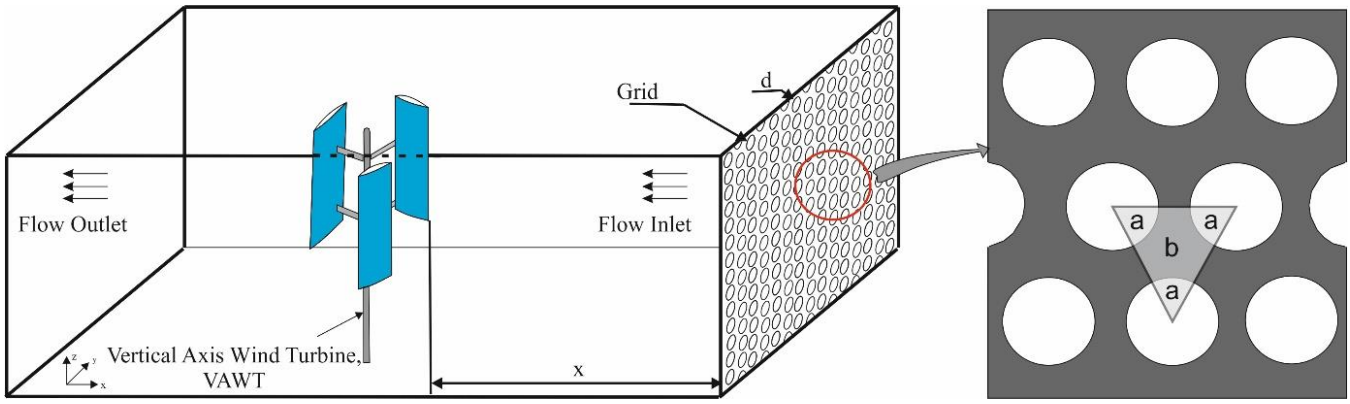

Fig. 5. Schematic representation of the test set-up and grid.

In order to calculate turbulence at first fluctuation flow velocity must obtained. Using this velocity value equation 2, Root Mean Square of these, u_{rms} is obtained and turbulence intensity can be calculated by equation (3).

$$\boldsymbol{u_{rms} = \sqrt{\sum_{i=1}^{n} \frac{(U_i - \overline{U})^2}{n-1}}} \qquad (2)$$

$$\boldsymbol{Tu(\%) = \frac{u_{rms}}{\bar{U}} \times 100} \qquad (3)$$

Where U is free stream flow velocity.

During the experiment effect of the solidity ratio, S was investigated and compared in figure 12 and figure 13 for S1014 and S1020 respectively.

2.3. Determination of DC motor efficiency

In order to determine the efficiency of the DC motor in the experiment, combine system was used as shown below in figure 6 at Nigde Omer Halisdemir University Lab. To explain the parts specified, number 1) Control panel, 2) Driver of the control panel, 3) Electronic load, 4) Data logger, 5) DC motor, 6) Torqumeter, 7) Laser Tachometer and 8) Electric motor. Figure 6b shows a detail illustration of the apparatus's overall perspective and is circled in red.

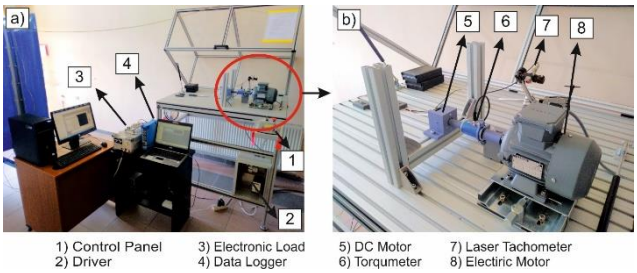

Fig. 6. Determination of DC motor efficiency set-up.

By changing the frequency through the control panel, the electric motor can be adjusted at the desired speed. In this step, motor rotation speed is set between 300 and 1800 rpm. The appropriate load is given according to the voltage value produced by the dc motor corresponding to each revolution. 10.000 number of samples were taken during the 10 seconds interval with 1000 sampling frequency per channel at the Oros data logger. These collected values were

averaged and an attempt was made to produce more precise and more accurate results. 5V input range was set to improve the accuracy of our results and 55P11, 1D probe was used to get only voltage as output.

3. RESULTS AND DISCUSSION

In this paper, the investigation of chord lengths, Angle of Attack, Aspect Ratio and presence of grid for the airfoils (S1014 and S1046) is done to get maximum output power from the wind turbine. When using two different airfoils, three different H/D ratios were formed with these blades, the blades connected to the system were tested at three different angles of attack with 0, 5 and 10 degrees and six different wind speeds varying between 4-9 m/s. Comparisons are made by repeating the same values of all these obtained values under turbulent flow.

The H/D for both blades in figure 7 can be regarded. At various flow velocities, this graph developed versus the coefficient of performance, Cp. As in this graph, complexity has been avoided by using the common value on the y axis in almost all other graphs. It is stated in figure 7 that as the H/D ratio increases, the performance coefficient increases, it is maximum at 1.5 and then decreases. The Cp value does not have a similar or specific relationship with the increase or decrease of wind speeds within the two wings. The only common situation is that it reaches its highest value at 1.5 H/D as mentioned earlier. Therefore, some graphs were created for 1.5 H/D ratio while other comparisons were made.

TSR versus Cp values were demonstrated in figure 8 at six different wind velocity. This comparison was made under the turbulence less than 1%. Although TSR (from 0.35 to 1.5) increases slightly as wind speed increases, the maximum Cp value has approximately the same values at 4, 5 and 6 m/s wind speeds. The highest Cp value was obtained at a speed of 8 m / s. In addition, wind speeds of 7, 8 and 9 m/s vary between 1 and 1.55 TSR for S1014. Similar trend applies to S1020. but has a lower performance curve than S1014. It has been observed that the Cp values change relatively less with the change of wind speed.

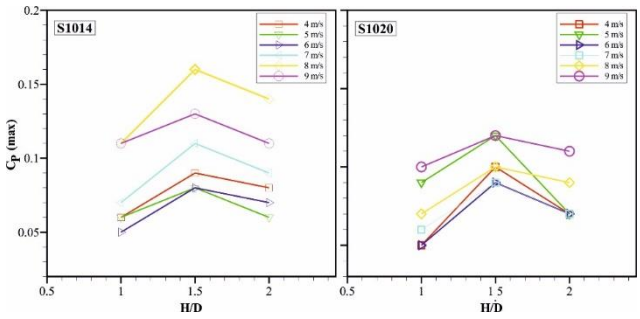

Fig. 7. Graphics of *H/D* ratios both *S1014* and *S1020* blade profile.

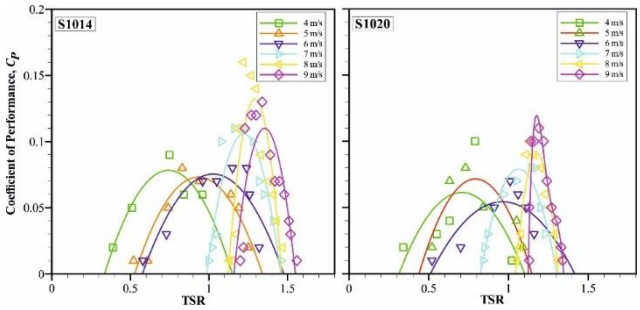

Fig. 8. Graphic of TSR versus Cp at different flow velocities.

Produced voltage, V (on the left), rotational speed, ω (in middle) and power, P (on the right) against to wind velocity for S1014 and S1020 were compared in figure 9 and figure 10 respectively. The red lines denoted by the square symbol in all figures indicate that turbulence is zero, and the green marked with a triangle means that turbulence corresponds to 5 percent. The purpose of expressing that turbulence is zero at this point and as shown in all graphs beyond is to express that it is below 1 percent. In other words, it is not working under zero turbulence, but a minimized state of turbulence in the wind tunnel. It is obvious that with increasing wind speed, all other outputs increase. Although the effect of turbulence seems to be small, change amounts are given for three separate points in the U∞-P graph.

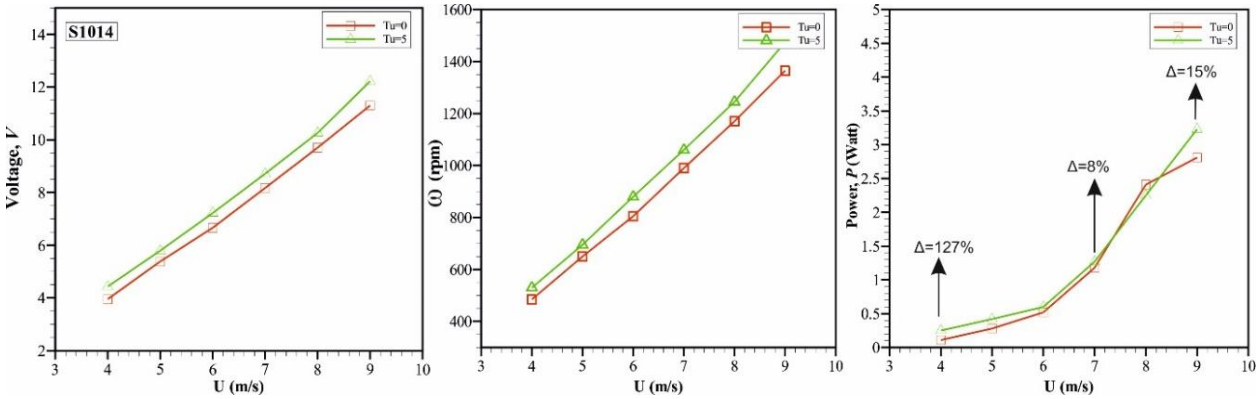

Fig. 9. Produced voltage, V, rotational speed, ω and power, P against to wind velocity for S1014.

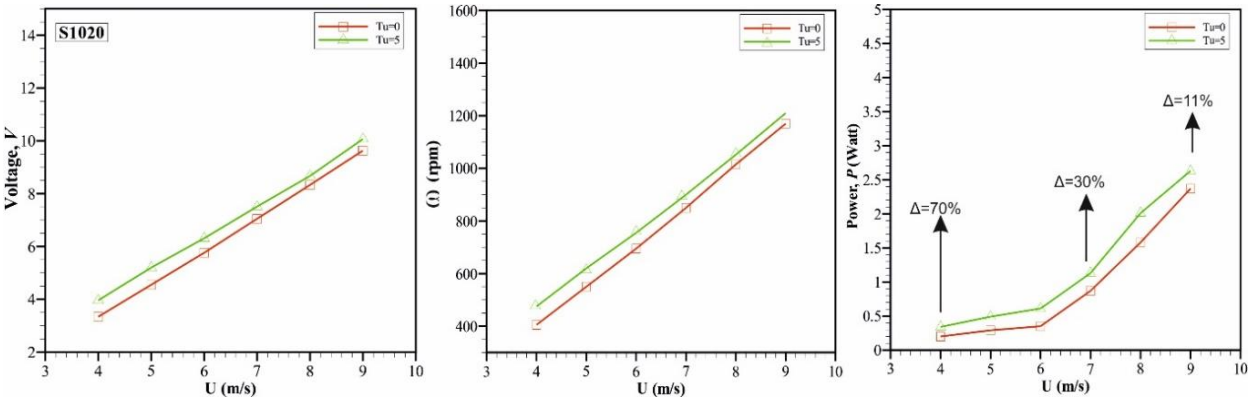

Fig. 10. Produced voltage, V, rotational speed, ω and power, P against to wind velocity for S1020.

In order to compare the power curves obtained under various angle of attack conditions, both turbulent and low turbulence conditions are plotted in Figure 11. S1014 blade profile is located on the left side of the graphic, while S1020 on the right. While the S1014 operates in the wider TSR range, the S1020 changes in the narrower. Increasing the turbulence for each velocity value has a positive effect on the performance coefficient. While the 5 and 10 degree of attack. Similar behavior was seen by S1014, although S1020 showed various differences, leading experts to conclude that 10 degrees was preferable. This is particularly evident at a free stream flow velocity of 8 m/s. Although the net Cp values at 8 m/s wind velocity are higher in S1014, the rate of increase is almost 23% and they are very close to each other.

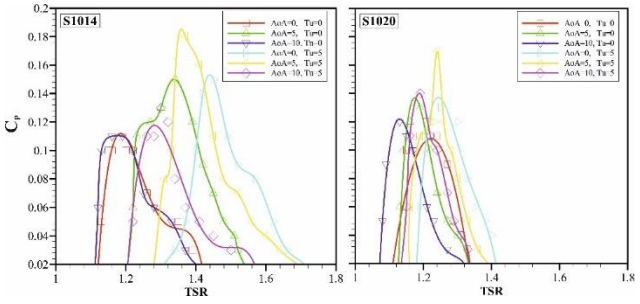

Fig. 11. Representation of TSR versus Cp according to Angle of Attack, AoA.

Figure 12 and figure 13 are related to the solidity ratio and is determined according to the aspect ratio. The effect of Solidity, S was evaluated by plotting the power curves for S1014 and S1020 in figure 12 and figure 13, respectively. Solidity of the wind turbine can be calculated from the equation 4 as shown below.

$$S = \frac{Nc}{\pi D} \qquad (4)$$

Where;

N is number of the blade, c is chord length and D is diameter of the turbine rotor.

It behaved differently at lower TSRs as a result of the increase in solidity. As can be understood from the turbulent situation with green lines and supporting figure 7, the maximum Cp was observed at S = 0.29, in other words at H/D=1.5. As the solidity rate increases in the S1020 profile, it shifts the operating range towards the lower region, although it does not narrow the working zone. Also proportionally, again at H/D = 1.5, there is the highest Cp change especially for S1020.

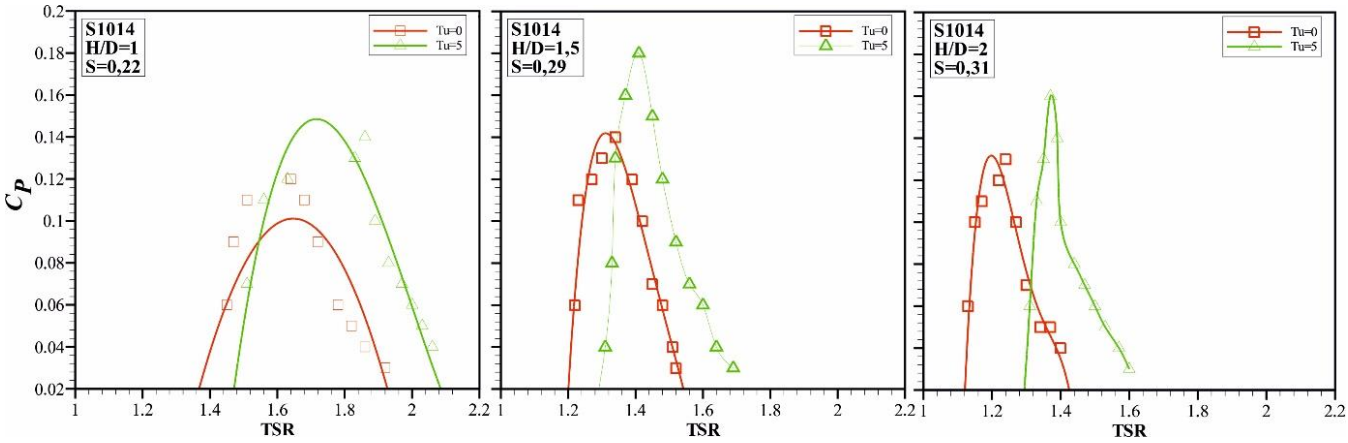

Fig. 12. Presentation of TSR versus Cp at different solidity for S1014.

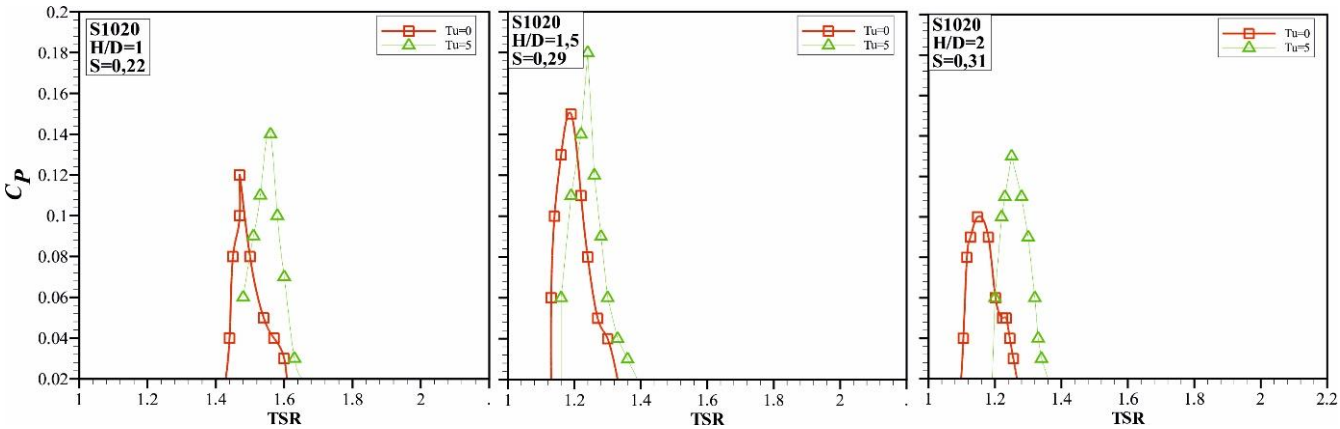

Fig. 13. Presentation of TSR versus Cp at different solidity for S1020.

Figure 14 contains all wind speed values (from 4 to 9 m/s) and allows comparisons with each other for both profile with presence of turbulence or not. To investigate the influence among the three parameters (turbulence, blade profile and wind velocity) only changes CP of each curve versus TSR is presented. green and red lines show S1014 while blue and turquoise colored lines represent S1020. It can be clearly seen that the increase in wind speed increases the Cp value, but it is observed that it does not change linearly when viewed as a ratio. Also, it is possible to obtain Cp close to 0.20 with increasing wind speed. At the same time, the increase in wind speed has narrowed the TSR range in which the turbine operates. As with all other graphs, this graph proves that the effect of turbulence is definitely positive for the performance coefficient. There is a dependence between Cp and TSR and it is an undeniable fact that turbulence has a positive effect on different blade models even though it has a different effect on this dependence.

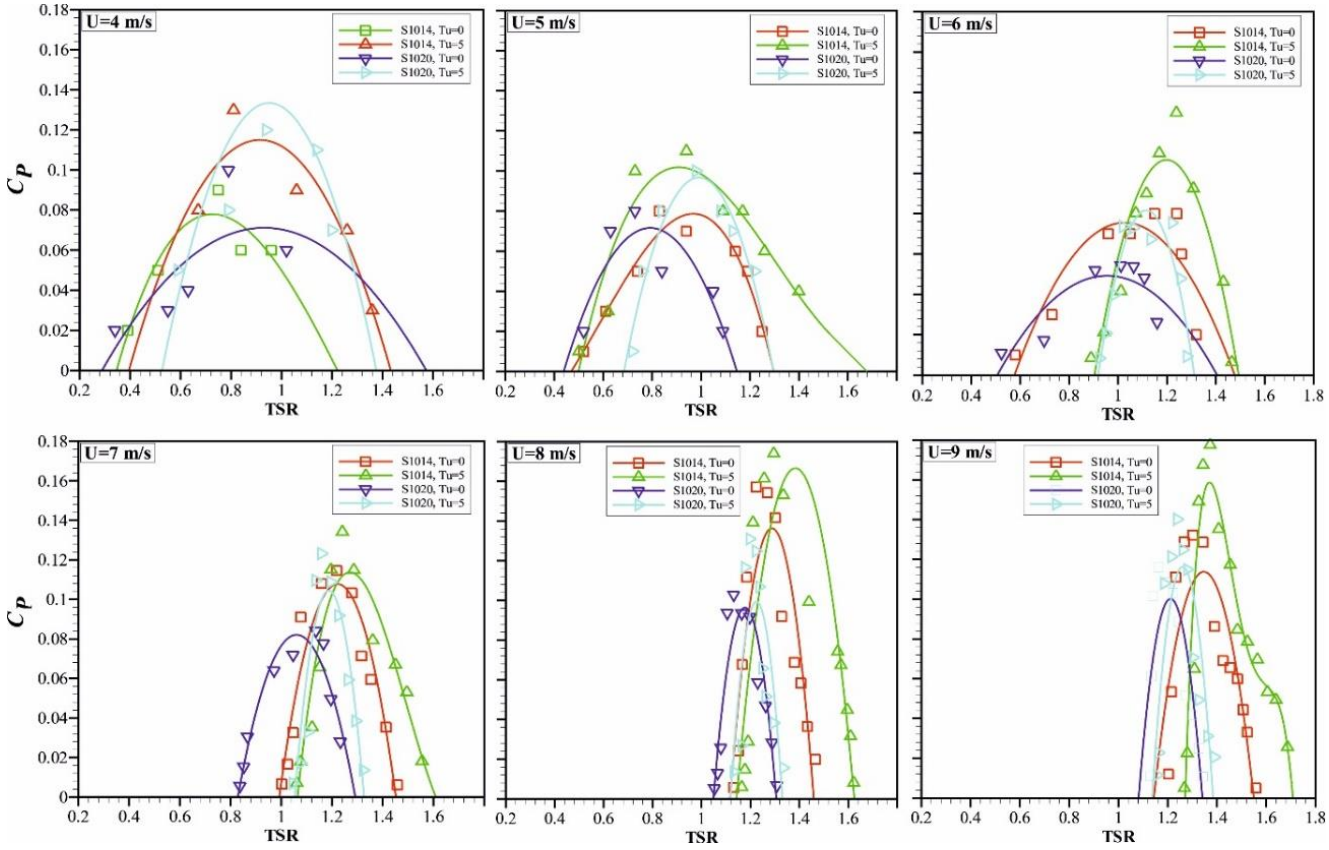

Fig. 14. Presentation of TSR versus Cp at different free stream flow velocity

4. CONCLUSION

Understanding the physics of air flow remains complex. Therefore, harvesting from wind energy could not reach the desired level. Researchers, engineers and scientists have many studies on this subject. If production and accessibility costs can be reduced rather than high performance, it will be seen among alternative and renewable energy sources in many parts of the world.

In this study, the performance of wind turbines designed according to two different blade profiles has been investigated by changing the different parameters in turbulent and low turbulence conditions. The findings obtained have been listed below.

i. Two different blade profiles called S1014 and S1020 were produced in the 3D printer and used in the turbine.
ii. The rotor diameter, D was changed by keeping the turbine height, H constant and three different H/D ratios were determined as 1, 1.5 and 2.
iii. Chord length was kept constant as 60 mm. Therefore, only aspect ratio influenced on solidity, S.
iv. Three different angles of attack, AoA=0, 5, 10 have been examined.
v. Six different free stream flow velocities ranging from 4 to 9 m/s have been set.
vi. The vortex generator with 52% porosity value, β was placed in the test area and all experiments were carried out both with low and high turbulence levels.
vii. For both blade types, the highest Cp value was observed at the level of H/D=1 and therefore at S=0.29.
viii. Overall, the S1014 performed better in almost most experiments.
ix. Since the grid used makes the flow on the turbine distorted, fluctuated and turbulent, it has increased the performance coefficient.

In the future, it is planned to examine the aerodynamic performances of the modified blade, and it is also planned to conduct studies in a wider sense using optimization algorithms.

Conflicts of Interest

There is no conflict of interest.

Acknowledgments

The present work is supported by The Scientific and Technological Research Council of Turkey, TUBITAK project no:315M478 and Erciyes University, FDK-2019-9685. The authors would like to thank their support.

Nomencleature

H	**:**	Height of Blade (mm)
D	**:**	Diameter of Turbine (mm)
D	**:**	Diameter of Grid Hole (mm)
H/D	**:**	Aspect Ratio (-)
x	**:**	Grid Distance (mm)
Cp	**:**	Power Coefficient (-)
λ	**:**	Tip Speed Ratio (-)
T	**:**	Torque (Ncm)
n	**:**	Number of Revolution (rpm)
S	**:**	Solidity (-)
Ls	**:**	Strut Length (mm)
U_{∞}	**:**	Free Stream Velocity (m/s)
ω	**:**	Angular Velocity (rad/s)
R	**:**	Radius of Turbine (mm)
D_C	**:**	Diameter of Connection Plate (mm)
D_h	**:**	Hole Diameter on Connection Plate (mm)
AoA	**:**	Angle of Attack (Degree)
C	**:**	Chord length of blade (mm)
β	**:**	Porosity (-)
u'	**:**	Fluctuation Velocity
Tu	**:**	Turbulence Intensity
u_{rms}	**:**	Root Mean Square of Velocity Fluctuation

REFERENCES

[1] Wekesa D. W., Wang C., Wei Y. and Danao L.A.M. 2014. "Influence of operating conditions on unsteady wind performance of vertical axis wind turbines operating within a fluctuating free-stream: a numerical study." *Journal of Wind Engineering Industrial Aerodynamics* 135 76–89.

[2] Li Y. and Willman L. 2014. "Feasibility analysis of offshore renewables penetrating local energy systems in remote oceanic areas- A case study of emissions from an electricity system with tidal power in Southern Alaska." *Applied Energy* 117(15):42–53. http://dx.doi.org/10.1016/j.apenergy.2013.09.032.

[3] Kumar R., Raahemifar K. and Fung A.S. 2018. "A critical review of vertical axis wind turbines for urban applications." *Renewable Sustainable Energy Review* 89:281–91. http://dx.doi.org/10.1016/j.rser.2018.03.033.

[4] Stathopoulos HA T., Al-Quraan A., Bert Blocken A.D., Paraschivoiu M., Pragasen P. 2018. "Urban wind energy: Some views on potential and challenges." *Journal of Wind Engineering Industrial Aerodynamics* 179:146–57.

[5] Wekesa D.W., Wang C., Wei Y., Kamau J. N., and Danao L.A.M. 2015. "A numerical analysis of unsteady inflow wind for site specific vertical axis wind turbine: a case study for marsabit and garissa in kenya." *Renewable Energy* 76 32–45.

[6] Scheurich F., Brown R.E. 2013. "Modelling the aerodynamics of vertical-axis wind turbines in unsteady wind conditions." *Wind Energy* 16 91–107.

[7] Sallah M.B., Kamaruddin N. M., Kassim Z. M. and Abu Bakar E. 2021. "Experimental investigation on the characterization of self-starting capability of a 3-bladed Savonius hydrokinetic turbine using deflector plates." *Ocean Engineering* 228 108950, https://doi.org/10.1016/j.oceaneng.2021.108950

[8] Kacprzak K., Liskiewicz G. and Sobczak K. 2013. "Numerical investigation of conventional and modified Savonius wind turbines." *Renewable Energy* 60 578–585.

[9] Ajedegba J. O. 2008. "Effects of blade configuration on flow distribution on flow and power output of a Zephyr vertical axis wind turbine." Ph.D. thesis. University of Ontario Institute of Technology.

[10] Pallotta A., Pietrogiacomi D. and Romano G. P. 2020. "HYBRI e A combined Savonius-Darrieus wind turbine: Performances and flow fields." *Energy* 191 116433, https://doi.org/10.1016/j.energy.2019.116433.

[11] Krishnan A. and Paraschivoiu M. 2016. "3D analysis of building mounted VAWT with diffuser shaped shroud." *Sustainable Cities and Society* 27:160–6. http://dx.doi.org/ 10.1016/j.scs.2015.06.006.

[12] Bhuyan S. and Biswas A. 2014. "Investigations of self-starting and performances of simple h and hybrid h-Savonius vertical axis wind rotors." *Journal of Energy Conversion and Management* 87 859–867.

[13] Biswas A., Gupta R. and Sharma K. K. 2007. "Experimental investigation of overlap and blockage effects on three-bucket Savonius rotors" *Journal of Wind Engineering Industrial Aerodynamics*. 31 363–368.

[14] Gupta R., Biswas A. and Sharma K. K., 2008. "Comparative study of three-bucket Savonius rotor with combined three-bucket-Savonius-three-bladed-Darrieus rotor." *Journal of Renewable Energy Aerodynamics* 33 1974–1981.

[15] Sengupta A. R., Biswas A. and Gupta R. 2016. "Studies of some symmetrical and unsymmetrical blade h-darrieus rotors with respect to starting characteristics, dynamic performances and flow physics in low wind streams." *Renewable Energy* 93 536–547.

[16] Jeon K. S., Jeong J. I., Pan J.-K. and Ryu K.W. 2015. "Effects of end plates with various shapes and sizes on helical savonius wind turbines." *Renewable Energy* 79 167–176.

[17] Laín S., Taborda M., and López O. 2018. "Numerical study of the effect of winglets on the performance of a straight blade Darrieus water turbine." *Energies* 11:297. https:// doi.org/10.3390/en11020297.

[18] Elkhoury M., Kiwata T. and Aoun E. 2015. "Experimental and numerical investigation of a three dimensional vertical-axis wind turbine with variable-pitch." *Journal of Wind Engineering Industrial Aerodynamics* 139:111–23. https://doi.org/10.1016/j.jweia.2015.01.004.

[19] Lin S., Lin Y., Bai C. and Wang W. 2016. "Performance analysis of vertical-axis-wind-turbine blade with modified trailing edge through computational fluid dynamics." *Renewable Energy* 99:654–62. https://doi.org/10.1016/j.renene.2016.07.050.

[20] Chen J., Chen L., Xu H., Yang H., Ye C. and Liu D. 2016. "Performance improvement of a vertical axis wind turbine by comprehensive assessment of an airfoil family." *Energy* 114:318–31. https://doi.org/10.1016/j.energy.2016.08.005.

[21] Mohamed M.H. 2012. "Performance investigation of H-rotor Darrieus turbine with new airfoil shapes." *Energy* 47:522–30. https://doi.org/10.1016/j.energy.2012.08.044.

[22] Zamani M, Nazari S., Moshizi S.A. and Maghrebi M.J. 2016. "Three dimensional simulation of Jshape-d Darrieus vertical axis wind turbine." *Energy* 116:1243–55. https://doi. org/10.1016/j.energy.2016.10.031.

[23] Takao M, Kuma H, Maeda T, Kamada Y, Oki M, and Minoda A. 2009. "A straight-bladed vertical axis wind turbine with a directed guide vane row – effect of guide vane geometry on the performance." *Journal of Thermal Science* 18:54–7. https://doi.org/10.1007/s11630-009-0054-0.

[24] Kim D and Gharib M. 2014. "Unsteady loading of a vertical-axis turbine in the interaction with an upstream deflector." *Experimental Fluids* 55:1658. https://doi.org/10.1007/s00348-013-1658-4.

[25] Jeon J. H. and Kim S. H. 2018. "Optimization of thick wind turbine airfoils using a genetic algorithm" *Journal of Mechanical Science and Technology* 32 (7) 3191~3199.

[26] Kim D. and Gharib M. 2013. "Efficiency improvement of straight-bladed vertical-axis wind turbines with an upstream deflector." *Journal of Wind Engineering Industrial Aerodynamics* 115:48–52. https://doi.org/10.1016/j.jweia.2013.01.009.

[27] Hashem I and Mohamed M.H. 2018. "Aerodynamic performance enhancements of H-rotor Darrieus wind turbine." *Energy* 142:531–45. https://doi.org/10.1016/j. energy.2017.10.036.

[28] Malipeddi AR, Chatterjee D. 2012. "Influence of duct geometry on the performance of Darrieus hydroturbine." *Renewable Energy* 43:292–300. https://doi.org/10.1016/ j.renene.2011.12.008.

[29] Dabiri J.O. 2011. "Potential order-of-magnitude enhancement of wind farm power density via counter rotating vertical-axis wind turbine arrays." *Review Science Instrumentation* 77:3A–303A. https://doi.org/10.1063/1.3608170.

[30] Zanforlin S, Nishino T. 2016. "Fluid dynamic mechanisms of enhanced power generation by closely spaced vertical axis wind turbines." *Renewable Energy* 99:1213–26. https://doi.org/10.1016/j.renene.2016.08.015.

[31] Parneix N, Fuchs R, Immas A, Silvert F. 2016. "Efficiency improvement of vertical-axis wind turbines with counter-rotating lay-out." Wind Europe Summit 2016.

[32] Yang Yang1 Chun Li, Wanfu Zhang, Xueyan Guo and Quanyong Yuan, 2017. "Investigation on aerodynamics and active flow control of a vertical axis wind turbine with flapped airfoil." *Journal of Mechanical Science and Technology* 31 (4) 1645~1655.

[33] Sagharichi A, Zamani M, Ghasemi A. 2018. "Effect of solidity on the performance of variable-pitch vertical axis wind turbine." *Energy* 161:753–75. https://doi. org/10.1016/j.energy.2018.07.160.

Research/Review Article *Energy, Environment and Storage* (2024) 04-01:13-17

Energy, Environment and Storage

Journal Homepage: www.enenstrg.com

The Future of 2D Materials Production: Graphene and Borophene on larger scale

Ryan Nadar[1], **Vijaya Kumar Varadarajan** [2]

[1]Researcher,Aerospace Engineering, Ajeenkya DY Patil University Pune ,India- *https://orcid.org/0009-0009-3717-9992*

[2] Dean of international division,Ajeenkya DY Patil University Pune , India - dean.international@adypu.edu.in

ABSTRACT. *The production of graphene and borophene, two distinct materials with remarkable properties, is investigated through the manipulation of charged ions in a plasma environment. Plasma, characterized by ionized atoms or molecules, offers a unique setting where diverse chemical reactions can take place. This research focuses on utilizing this environment to create longer-chain graphene and carbon nanotubes by manipulating charged carbon ions. When positively and negatively charged carbon ions coexist within the plasma, they have the potential to interact and form bonds. This interaction results in the growth of extended carbon structures, particularly graphene. By carefully controlling plasma conditions such as temperature, pressure, and composition, scientists can guide the formation of longer-chain graphene and carbon nanotubes from these charged carbon ions. Similarly, the production of borophene, a material composed of boron atoms, also takes place in a plasma state. By introducing positively and negatively charged boron ions into the plasma, these ions interact and potentially form bonds, leading to the growth of extended borophene structures. This innovative approach unlocks the potential for tailored materials with enhanced property*

Keywords: *Graphene ; Borophene ; Atomic-level manipulation ; Charge Particle ; Scalable production*

Article History: Received: 02.01.2024; Accepted: 29.01.2024

Doi*:* **https://doi.org/10.52924/VFXC5133**

1. INTRODUCTION

The Production of graphene and borophene, two extraordinary materials renowned for their exceptional properties, has become a focal point in scientific inquiry. Scientists, seeking innovative approaches to their production, have delved into the intriguing realm of plasma, where ionized atoms or molecules create a distinctive environment conducive to diverse chemical reactions. Graphene, a two-dimensional lattice of carbon atoms, boasts remarkable mechanical, electrical, and thermal properties, holding immense promise for various applications. This study concentrates on generating longer-chain graphene and carbon nanotubes by manipulating charged carbon ions within a plasma. The interplay between positively and negatively charged carbon ions facilitates bond formation, fostering the growth of extended carbon structures. In the case of borophene, a material composed of boron atoms, it has recently emerged as a captivating subject for scientific exploration. Researchers aim to exploit the plasma state of boron, where both positively and negatively charged boron ions coexist, to encourage potential bond formation between these ions. This interaction within the plasma environment creates an opportunity for the development of extended borophene structures. In employing plasma-based techniques for synthesizing these extraordinary materials. The use of plasma as a medium provides several advantages, including precise control over the growth process and the ability to produce unique structures that are challenging to achieve through conventional methods. To further explore this captivating field, researchers are investigating various aspects of plasma-based synthesis, such as optimizing plasma parameters, controlling ion energy, and experimenting with different precursor molecules. These endeavors aim to unlock the full potential of plasma-enabled material synthesis, paving the way for groundbreaking applications in electronics, energy storage, and beyond. Furthermore, the versatility of plasma-based synthesis extends beyond graphene and borophene. This research holds the promise of revolutionizing the landscape of advanced materials, driving innovation across numerous industries.

2. MATERIALS AND METHODS

For the successful implementation and elucidation of this concept, reliance on information from peer-reviewed journals and pertinent websites is essential to provide a

comprehensive explanatory perspective. The scaling up of graphene and borophene production is achieved by altering the charged particles at the atomic level. Both materials are synthesized on a larger scale by manipulating their charged particles in a plasma environment, facilitating unique chemical reactions. Specifically, in the production process of graphene, carbon ions within the plasma are manipulated to generate graphene structures. The plasma state, where atoms exist as either positive or negative, is leveraged by inducing ionization to create positive or negative carbon and boron ions. A potential difference is also applied to establish distinct positive and negative regions. Carbon atoms, present in the plasma state, undergo manipulation, enabling the formation of extended carbon structures, such as graphene or carbon nanotubes. When positively and negatively charged carbon ions coexist in the plasma, they have the potential to form bonds, fostering the growth of larger carbon structures. This controlled manipulation of charged carbon ions in the plasma facilitates the creation of extended graphene and carbon nanotube chains. Similarly, the production of borophene involves a plasma environment where boron atoms, in the plasma state, coexist as positively and negatively charged ions, allowing for interaction and bond formation. By manipulating these charged boron ions, extended borophene structures can be synthesized. It is important to note that the explanation provided is currently within a theoretical framework, offering a novel approach for the scalable production of graphene and borophene.

3. Literature review

For both graphene and borophene, a similar process is used for their production. When carbon is used to produce graphene, first, carbon is heated to a very high temperature. During this process, copper or another substrate is used, and the carbon at high temperature adheres to the surface of the copper. This results in the formation of a layered structure for graphene. Similarly, for borophene, a similar method is employed. Boron is heated at high temperatures, and it bonds to a gold substrate. This bonding process on the gold substrate leads to the formation of borophene. It's important to note that while the production processes are similar due to use of substrate but are very different process to make it, graphene and borophene are two very different materials.

CVD is a widely used technique for synthesizing graphene, a two-dimensional carbon allotrope with remarkable electronic, thermal, and mechanical properties. The process involves introducing precursor gases onto a substrate, where carbon atoms are deposited to form a graphene layer.

Substrate Selection: The choice of substrate is crucial for the quality and properties of the resulting graphene. Common substrates include copper, nickel, and silicon carbide.

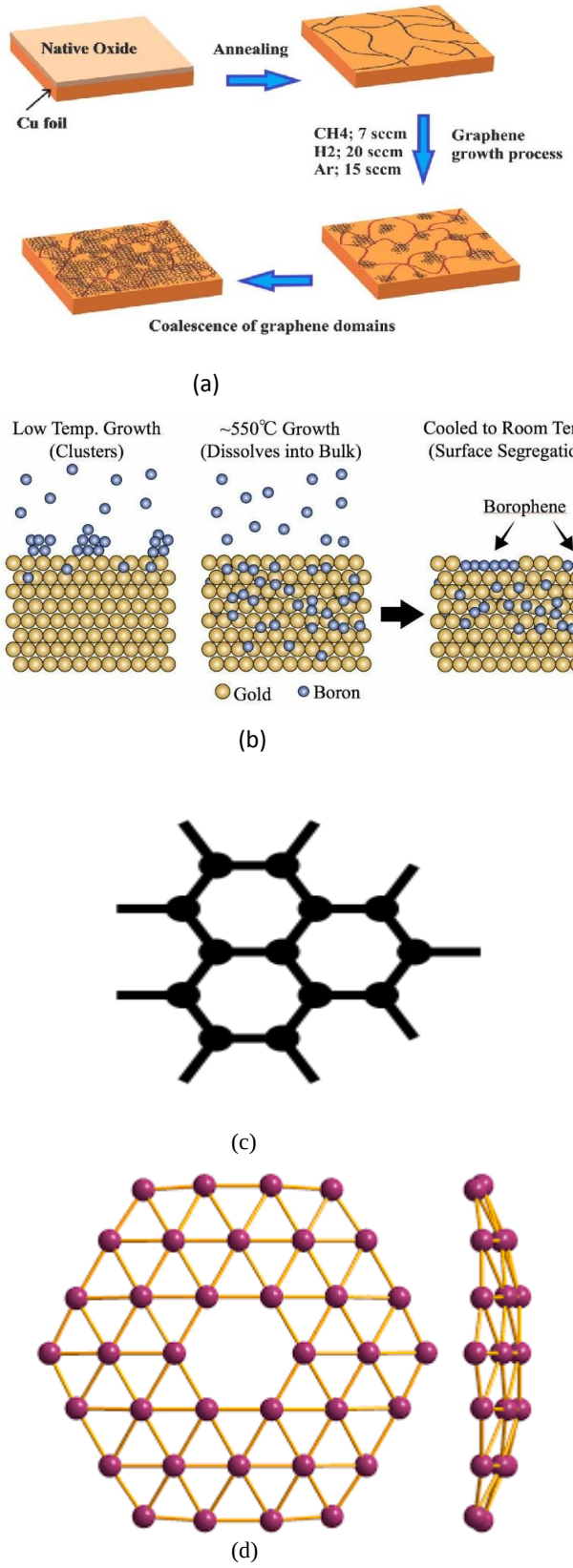

Figure 1. (a) Graphene production by using chemical vapor deposition (CVD) substrate of copper; (b) Borophene production by physical vapor deposition (PVD); (c) Graphene; (d) Borophene

Precursor Gases: Methane or ethylene is often used as carbon precursor gases in CVD processes. The choice of the precursor affects the growth rate and quality of graphene.

Temperature and Pressure: Optimizing temperature and pressure conditions is essential for controlling the growth kinetics and structure of graphene. Low-pressure CVD is commonly employed for large-scale production.

Catalysts: Catalysts such as copper foil or films are commonly used to facilitate the growth of graphene. The choice of catalyst influences the nucleation and growth of graphene layers [9].

Advances and Challenges: Recent research has focused on enhancing the scalability, reproducibility, and cost-effectiveness of CVD graphene production. Challenges include achieving high-quality, single-layer graphene over large areas and minimizing defects.

Borophene Production: Overview: Borophene is a 2D sheet of boron atoms with unique electronic and structural properties. Its production involves similar techniques as graphene but with specific considerations due to boron's different bonding characteristics.

Key Considerations: Substrate and Growth Surface: Substrates like silver and copper are often used for borophene growth. The choice of substrate influences the stability and structure of borophene.

Precursor Molecules: Boron precursors are typically used, and the selection of precursor molecules impacts the growth kinetics and properties of borophene.

Temperature and Atmosphere: The growth temperature and atmosphere play a crucial role in determining the stability and crystalline structure of borophene.

Post-Processing Techniques: Various post-processing techniques are employed to transfer borophene from the growth substrate to desired target substrates while maintaining its integrity.

Advances and Challenges:

Borophene is a relatively new material, and research is ongoing to understand its properties and potential applications. Challenges include achieving large-scale production and developing techniques to control the synthesis of different borophene polymorphs.

For Graphene Production chemical vapor deposition (CVD):Layers of graphene will form on the copper's surface from the plentiful carbon atoms in the methane gas, a process called chemical vapor deposition (CVD) [1]whereas Brophene production by physical vapor deposition (PVD) :when heated in a furnace and place on a gold surface, boron atoms dissolve into a bath of gold and when the materials cool down, they resurface in the form borophene [2],Overall, in both cases, one thing is the same for all, and that is to make borophene and graphene by using substrate.

4. Research overview

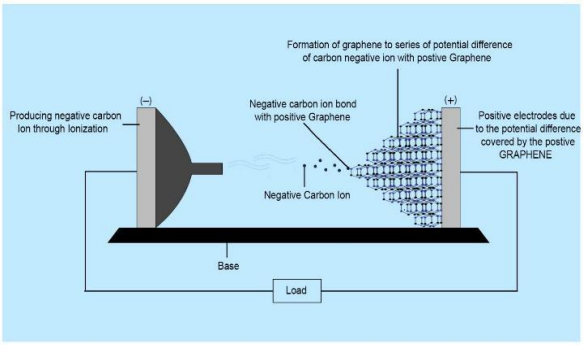

(e)

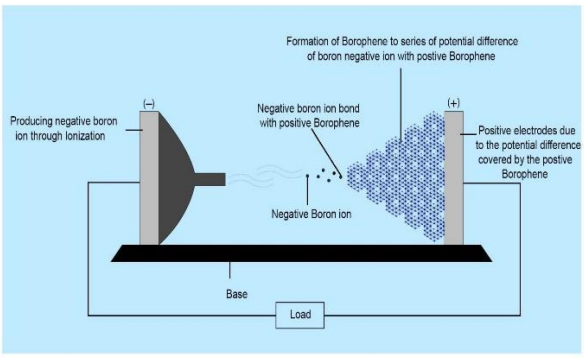

(f)

Figure 2. (e) Graphene production by negative carbon ion bonding with positive carbon; (f) Borophene production by boron negative ion bonding with positive boron.

In this research work, there are two of the The production of graphene and borophene, two remarkable materials with exceptional properties. By same method by which atom is in plasma stage change their charge particle in which opposite charge attract by which form a long chain of it When in plasma stage (ionization) the atom is become negative due to ionization of it - a small of part of atom which already a graphene or borophene is become positive because of energy potential difference energy applied to it , Ionization (charge of charged particle) Adiabatic ionization : Ionization is the process by which ions are formed by gain or loss of an electron from an atom or molecule. If an atom or molecule gains an electron, it becomes negatively charged (an anion), and if it loses an electron, it becomes positively charged (a cation). Energy may be lost or gained in the formation of an ion [3] , During this process of making graphene and borophene, overall it will lead to continuous bonding where a negative carbon ion bonds with a positive carbon, resulting in the formation of graphene. Similarly, a negative boron ion will bond with a positive boron ion, leading to the creation of borophene

In graphene production, both negative carbon ions and positive carbon ions can be created electrically. Similarly, in borophene production, negative boron ions and positive boron ions can be made from borophene. In both cases, the generation of positive and negative ions is due to the potential difference in charged particles,

Potential difference is the difference in the amount of energy that charge carriers have between two points in a circuit [4] & The difference in charge between higher potential and lower potential is called a voltage or potential difference [5]. But the difference is in the format; one stage will be in a plasma state, and another will be in a solid state due to potential differences. From that perspective, the chemicals are of the same element but have different charged particles that bond, Opposite charges attract both within the same atom and between atoms. This attraction forms chemical bonds between different elements [6].

An ion is an atom or group of atoms in which the number of electrons is not equal to the number of protons, giving it a net positive or negative electrical charge [7]. The presence of charged particles makes plasma electrically conductive, with the dynamics of individual particles and macroscopic plasma motion governed by collective electromagnetic fields and very sensitive to externally applied fields [8].

For graphene as per the figure 2 (e): Plasma, consisting of ionized atoms or molecules, serves as an intriguing medium for graphene production. In this process, carbon atoms are introduced into a plasma environment, where they become charged carbon ions. This plasma environment provides a highly reactive atmosphere, enabling various chemical reactions to occur. The presence of charged carbon ions within the plasma opens up the possibility of manipulating and controlling their behavior to induce specific reactions, one of the key aspects of plasma-based graphene production is the coexistence of both positively and negatively charged carbon ions within the plasma. These charged carbon ions have the potential to interact with each other, facilitating bond formation and the subsequent growth of extended carbon structures, including graphene and carbon nanotubes. By manipulating the trajectories and energies of these charged ions, researchers can guide their interactions and promote the formation of desired carbon structures. The ability to create longer-chain graphene structures and carbon nanotubes through plasma manipulation holds significant promise. By carefully controlling the plasma parameters, such as gas composition, pressure, and energy input, this level of control provides opportunities for tailoring the properties of graphene, such as its electrical conductivity, mechanical strength, and thermal stability, to suit specific applications. The advantages of plasma-based graphene production lie in the unique environment it offers. Plasma provides a versatile platform for generating a wide range of chemical reactions, allowing for the synthesis of graphene and related carbon structures. Moreover, the ability to manipulate charged carbon ions within the plasma enables precise control over the growth process, leading to the formation of extended carbon structures with desired characteristics. In summary, research in plasma Ionization -based graphene production focuses on utilizing the reactive environment of plasma to manipulate charged carbon ions and facilitate the growth of extended carbon structures. By controlling the interactions and potential bond formations between positively and negatively charged carbon ions, researchers aim to create longer-chain graphene structures

For Borophene as per the figure 2 (f) : similarly , the Borophene will be produced in longer format .In the plasma(ionization) -based approach for borophene production, boron atoms are introduced into a plasma environment, where they enter a charged state, becoming positively and negatively charged boron ions. The plasma state offers a conducive environment for chemical reactions, facilitating the interaction of these charged boron ions and potential bond formation-which will make a borophene where the ions are often near the ambient temperature while electrons reach thousands of kelvin [10].

The advantages of plasma (ionization)-based borophene production lie in the unique environment that plasma provides. Plasma serves as a reactive medium where boron ions can interact and form bonds, leading to the growth of extended borophene structures. The ability to manipulate charged boron ions within the plasma offers researchers a means to precisely control the growth process, resulting in the production of borophene with desired properties

Overall the research work is to make a contioous bond of same element by change their charge particle by particle via electrical mean, which mean that there is no need of substrate to produce a borophene and graphene, since substrate reduces the properties of graphene and borophene, such as the substrate can affect the band gap of graphene, which can make it less useful for certain applications. Also, to remove the substrate, various chemical processes are needed, and this will lead to a more expensive production of graphene and borophene

5. Results

In the manufacturing of graphene and borophene, we've established that a substrate is dispensable. Instead, we employ carbon gas, which assumes a negative charge in the plasma stage, to establish bonds with graphene in a sodiated state. Likewise, boron gas, also attaining a negative charge in the plasma stage, can form bonds with sodiated borophene. The manipulation of charges is achieved by controlling the potential difference during the ionization of plasma gas atoms, converting them into negatively charged entities conducive to bonding with sodiated graphene and borophene.

6. Discussion

Plasma Generation and Control: One of the primary challenges in the production of graphene and borophene using plasma is the generation and control of the plasma itself. Creating and maintaining a stable plasma environment with the desired properties requires careful control of parameters such as gas composition, pressure, temperature, and energy input. Achieving optimal plasma conditions for the growth of graphene and borophene structures can be a complex task that requires advanced plasma generation techniques and precise control mechanisms.

Challenges: The plasma stage occurs during ionization, transforming the atom into a highly charged particle stage. Ionization generation requires a magnetic field for control and the ability to bond graphene or borophene. Higher temperatures are also necessary for proper control, including managing excess heat.

Benefits: No substrate is required for chemical bonding because bonding is achieved through charge manipulation. Various chemical processes are not needed, making graphene and borophene production simple and easy.

7. Conclusion

The application of a plasma environment in the synthesis of graphene and borophene creates a versatile platform that allows precise control over the growth and characteristics of these materials. By manipulating charged carbon or boron ions within the plasma, interactions and bond formations are facilitated, leading to the creation of extended structures like graphene or borophene. This pioneering approach shows great potential for achieving scalable production of high-quality graphene, carbon nanotubes, or customized extended borophene structures. These advancements carry substantial implications for a wide range of applications, including electronics and energy storage, ushering in groundbreaking developments in materials science and technology.

Author contributions

Ryan Nadar is a researcher currently focused on multiple sectors, including Energy, Propulsion, Materials, and Software-Based Platforms. He is pursuing a degree in Aerospace Engineering at Ajeenkya DY Patil University in Pune, India. Additionally, Mr. Vijaya Kumar Varadarajan serves as the Dean of the International Division at Ajeenkya DY Patil University in Pune, India. He has been instrumental in assisting Ryan Nadar by providing various links to conferences, events, and other topics relevant to his research work. Importantly, Vijaya Kumar Varadarajan has been a research advisory for Ryan Nadar, guiding him through conference formats, helping with the publication of his research work, and facilitating collaboration opportunities at both the international and national levels. This paper was primarily authored by Ryan Nadar, and Ryan Nadar is the owner of this work.

Funding

The research is funded by Emergent Ventures, a division of EV India, with a grant amount of $4,500 awarded to Ryan Nadar. The funding has been allocated for research in the Energy Sector, as well as other sectors such as Propulsion, Materials, and Software-Based Platforms. Ryan aims to leverage these resources to enhance the intensity and global outreach of his research work.

Acknowledgments

Ryan Nadar is immensely grateful to two individuals and organizations, namely, Vijaya Kumar Varadarajan and Emergent Ventures Mercatus center. Vijaya Kumar Varadarajan provided valuable conference links, enabling Ryan to effectively communicate his research findings. On the other hand, Emergent Ventures has been instrumental in sharing Ryan's research work with the global academic community and funding for Graphical representation work.

Conflict of interest

The main reason why Ryan Nadar has shown interest in graphene and borophene is that in the future, it will be produced without needing a substrate, reducing various chemical processes as well as production costs. This will be useful in various platforms such as the Electronics Industry, Energy Storage, Aerospace and Aviation, Medical Devices, Water Purification, Flexible Electronics, Automotive Industry, Coatings and Composites, Solar Panels, Construction, and many more

References

1. LESJOHNSON,JOSEPHE.MEANY.n.d.MassProducingGraphene.URL:https://www.americanscientist.org/article/mass-producing-graphene#:~:text=Layers%20of%20graphene%20will%20form,produced%20is%20not%20very%20good
2. Valentina Ruiz Leotaud.Researchers learn to produce borophene on a gold surface.31 March 2019.URL:https://www.mining.com/researchers-learn-produce-borophene-gold-surface/#:~:text=Scientists%20from%20Rice%20University%2C%20Argonne,atom%2Dflat%20form%20of%20boron
3. UPAC. (1997). Compendium of Chemical Terminology, 2nd ed. (the "Gold Book"). Online corrected version: (2006–). "adiabatic ionization." doi:10.1351/goldbook.A00143
4. Potential Difference .n.d.URL: https://senecalearning.com/en-GB/definitions/potential-difference/#:~:text=Potential%20difference%20is%20the%20difference,two%20points%20in%20a%20circuit
5. SANTOSH DAS.Potential Difference. 28 JULY 2021 .URL: https://www.google.com/search?q=Why+is+it+called+potential+difference%3F&sourceid=chrome&ie=UTF-8
6. What are chemical bonds.n.d. URL:https://www.ferrovial.com/en/stem/chemical-bonds/#:~:text=Ionic%3A%20this%20occurs%20when%20metallic,attraction%20between%20their%20opposite%20charges
7. Chemistry Talk. (n.d.). Examples of Cations and Anions. Chemistry Talk. https://chemistrytalk.org/examples-of-cations-and-anions/#content
8. Morozov, A.I. (2012). Introduction to Plasma Dynamics. CRC Press. p. 30. ISBN 978-1-4398-8132-3.
9. Ji, E., Kim, M. J., Lee, J.-Y., Sung, D., Kim, N., Park, J.-W., Hong, S., & Lee, G.-H. (Year). Substrate effect on doping and degradation of graphene. Journal Name, Volume(Issue),DOI : https://doi.org/10.1016/j.carbon.2021.08.048
10. Hamrang, Abbas (2014). Advanced Non-Classical Materials with Complex Behavior: Modeling and Applications, Volume 1. CRC Press. p. 10

Research Article *Energy, Environment and Storage (2024) 04-01:18-24*

Energy, Environment and Storage

Journal Homepage: www.enenstrg.com

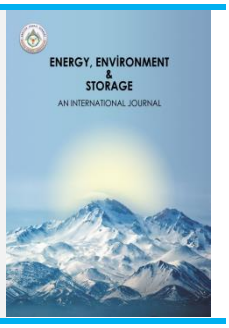

Training on Creating Learning Media to Improve the Ability to Create Learning Media Kamishibai for Environmental and Disaster Education

Indriyani Rachman[1,2], Irvan Permana[2], Lilis Siti Hindun[2], Mutia Sri Rahayu[2,] Yasmine Hadiastriani[2], Murae Fumitoshi [3] Yayoi Kodama[4]

[1]Faculty of Environmental Engineering, Graduate School of Environmental Engineering The University of Kitakyushu, Kitakyushu, Japan, ORCID: 0000-0001-7511-6241
[2] Postgraduate Program, Science Education, Universitas Pakuan Indonesia
[3] Disaster Mitigation Department, The University of Kitakyushu
[4]Department of Social Studies, Faculty of Humanities, The University of Kitakyushu

ABSTRACT

Indonesia is a country that is prone to disasters caused by environmental damage; therefore, community preparedness in facing disasters must start early. Bogor Regency is a city with very high rainfall; flash floods and landslides often occur in this area. The geographical contours of the Bogor district area are hilly and mountainous, making landslides frequent. Environmental education and disaster mitigation are efforts to provide knowledge to the broader community. With environmental education and disaster mitigation, it is necessary to disseminate learning methods that can be taught to students at school. In this training, attended by 17 teachers at SMP Negeri 2 Caringin, Bogor Regency, the participants took part in training on creating learning media to teach environmental impacts and disaster mitigation. This teaching media was adopted from learning media in Japan, namely Kamishibai. The participants were given socialization about Kamishibai, how to create scenarios, take pictures and present them. Data was collected through questionnaires and narratives created by participants. From the data collection results, participants felt they had new knowledge and abilities in creating learning media for environmental education and disaster mitigation. Participants also thought that Kamishibai media was exciting and made teaching easier for teachers. Kamishibai's scenario narrative was calculated using cloud words, counting the words that emerged from the narrative compiled by the training participants; landslides, floods, earthquakes, and rubbish were the words that dominated the other words.

Keywords: Environmental Education, Disaster education, Disaster mitigation learning media, Mitigation training

Article History: Received: 05.01.2024; Accepted: 30.01.2024

Doi: https://doi.org/10.52924/CHDK6603

INTRODUCTION

Caringin District is one of 40 (forty) Districts in Bogor Regency with an area of 5,729.9 Ha, located at 556 above sea level, humidity with an average temperature of 27–30^{0}C and rainfall of 3,183 mm/year. The hydrometeorological disaster triggered landslides, floods and fallen trees in Bogor district, West Java, for two days, 11-12 October 2022. This natural disaster caused by high-intensity rainfall also caused fatalities and injuries. Meanwhile, the Meteorology, Climatology and Geophysics Agency (BMKG) noted that the West Java region will still be hit by extreme weather and potential hydrometeorological disasters such as strong winds, heavy rain, floods, flash floods and landslides until the following week (27 December 2023 - 3 January 2024). During 2010 - 2020 in Indonesia, hydrometeorological disasters frequently occurred, especially landslides due to deforested forests, tornadoes, and floods. As a result of climate change, hydrometeorological disasters can occur. Caringin District is one of the Bogor Regency areas at risk of hydrometeorological disasters.

Environmental problems are related to deforestation, causing further environmental damage and triggering natural disasters. How must society protect the environment to reduce the possibility of natural disasters, landslides, and floods?

Early disaster prevention is necessary to overcome the increase in disaster victims in the Bogor Regency area. Disaster literacy through environmental and disaster education is one effort that can be made. This is also supported by the regional government, which states that there is a need to strengthen disaster knowledge or literacy among the community, especially those who live in disaster-prone areas, for example, people who live around the slopes of the highlands.

Efforts to reduce disaster risk require good disaster management and an orderly system. Education should be integrated with the education sector and school subjects. Many disaster victims are children under the age of 15 years and under. Many are victims of disasters, and many experience stress and trauma. This negative impact can be reduced by providing knowledge about natural disasters and training students in dealing with natural disasters.

The school community, including students, teachers, parents, and communities around disaster-prone areas, need to receive environmental education and natural disaster mitigation from an early age to reduce the impacts that occur after natural disasters. One strategy can be implemented through conservation education to increase knowledge, behavior, and attitude in environmental education and community skills related to surrounding natural resources' positive and negative impacts. This is also supported by previous researchers who said that knowledge about natural disasters and the impacts they cause, both positive and negative, needs to be understood by the public. This research aims to produce environmental education and disaster mitigation media that can be used as supporting material for teaching disaster mitigation.

Figure 1. Map Indonesia and Bogor

Education about awareness of natural disasters has been carried out since children are in daycare at school up to university level. At every level of education, they are periodically given training in dealing with disasters and disaster evacuation. This is one of the actions taken because Japan is a disaster-prone country; Japan has a long record of disasters. In the disaster SOP, the government requires that every building erected must be earthquake-resistant because Japan is a country that is often hit by earthquakes. The learning method regarding preventing natural disasters in Japan has been tested. Therefore, teaching and introduction methods for disaster mitigation were tested in Bogor.

2. MATERIALS AND METHODS

2.1. Design of Research

This research involved 20 teachers at SMP Negeri 2 Caringin, Bogor Regency. Give consent to participate in training and testing of environmental education and disaster mitigation learning media using methods commonly used in schools in Japan. The design is longitudinal, including pre-and post-training assessments and testing. This training plan and learning trials are teacher capability development carried out as part of a disaster education research program using kamishibai.

2.2. Overview of the Research Program

The training and trial program will be implemented in December 2023 at SMP Negeri 2 Caringin Bogor. Training participants were given training about Kamishibai and how to use it. Then, examples of cards with natural disaster themes are given earthquakes and floods caused by heavy rain. After debriefing, participants are trained to create scenarios about the storyline that the participants will create. Then, sketch the story. When creating a story, it consists of 5 cards, consisting of the first page in the form of a cover, cause, effect, and problem-solving.

2.3. Evaluation of the Research Programs

The participants carry out activities to create media according to the directions and flow determined to produce a communicative Kamishibai. Even though the participants were initially unsure, they could take good pictures. However, Kamishibai is a medium that does not require good images but conveys the message in a more prioritized way. Teacher collaboration as a group creates maximum Kamishibai love. The presentation was well done and focused. Below is the training research scheme flow for making disaster mitigation learning media, Kamishibai.

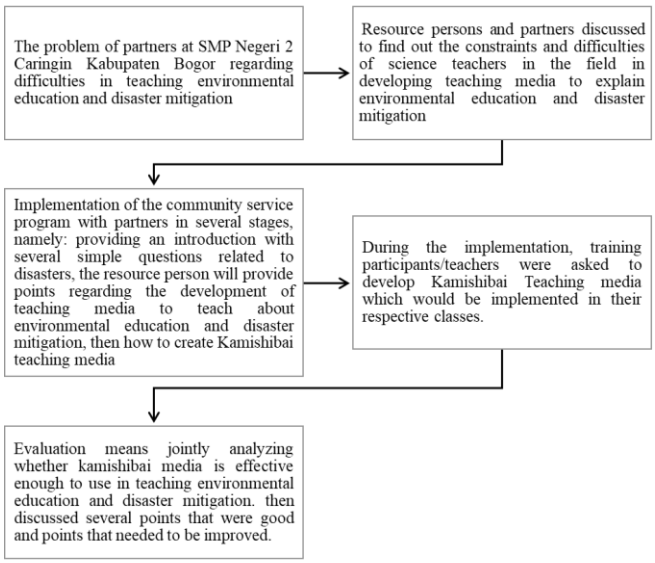

Figures 2. Research flow of Kamishibai media creation

2.4. Statistical Analysis research

In this training, participants were given a questionnaire regarding the benefits of taking part in training to create disaster mitigation learning media in the form of kamishibai, after which data was also taken based on stories created by participants in groups, then processed using a word cloud to count how many words appeared.

3. RESULT

3.1 Flow of training activities

The activity, which 17 participants attended, was carried out at SMP Negeri 2 Caringin and went smoothly; all participants followed directions and produced four sets of Kamishibai with the theme of disaster mitigation, ready to be tested on each student. Below, in Figure 3, is a photo of the activities of the training participants according to the flow of making Kamishibai.

Figures. 3. Photos of training participants' activities

3.2 Results of questionnaire distribution analysis

Participants were given a questionnaire after participating in the Kamishibai-making activity, the results of which were that participants felt they had new knowledge related to learning media. Participants also felt that it was essential to teach disaster mitigation education to students; using Kamishibai, teaching disaster mitigation was more effective. Kamishibai is an exciting medium to use, and participants hope that many other teachers will participate in this training because it is beneficial. Table 1 shows the results of participants' answers regarding their teaching media training experience.

3.3 Results Analysis of Kamishibai's narrative

Figure 4 shows the words from the Kamishibai storyline compiled by the training participants. From three set kamishibai with different themes, namely deforestation, rivers and rubbish and volcanic eruptions, 450 words were collected from 3 kamishibai narratives. Then, use cloudword and cut words that are under four words. So, you get the words in Figure 4 and Table 2 below. Rivers, rubbish and floods are mentioned most often in the narrative.

Table 1. Results of distributing questionnaires to training participants

Quesioner	Workshop participant number																
	1	2	3	4	5	6	7	8	9	10	11	12	13	14	15	16	17
In my opinion, teaching disaster education is very important	5	4	1	5	5	5	5	5	5	5	5	5	5	5	5	5	5
Teaching disaster education using learning media is more effective	5	4	5	5	5	5	5	5	5	5	5	5	5	5	5	5	5
Kamishibai media can be a tool for teaching disaster education	5	4	5	5	4	5	5	5	5	5	5	5	5	5	5	5	5
Kamishibai's teaching media is interesting enough to be used as a learning medium for disaster education	5	4	5	2	4	5	5	5	5	5	5	5	5	1	5	5	5
I hope that many teachers will have the opportunity to take part in workshops or training regarding disaster education	5	4	5	5	4	5	5	5	5	5	5	5	5	5	5	5	5

Figure. 4. Thema dan Kamishibai

Table. 2 The number of words that appear

Word list	Total number of words	The number of words that appear
River	450	13
Rubbish	450	12
Floods	450	9
Residents	450	7
Forest	450	6
People	450	6
Landslides	450	5
Village	450	5
Causes	450	4
Clean	450	4
Flooding	450	4
Waste	450	4

3.4 Results of the work of training participants

3.4.1 Group 1, Title: forest causes flooding

Kamishibai Narrative: Bare Forest Causes Floods
In a forest, illegal logging occurs by cutting down trees in the forest by irresponsible people. The forest becomes bare and feels very hot; this causes the land to be unable to hold water when it rains and causes floods and landslides; residents' houses are submerged due to flash floods from the denuded forest. Residents affected by the flood ended up living in evacuation posts. The community has realized that barren forests can cause floods and landslides; reforestation must correct this. Residents work together to plant new trees in the forest to prevent flooding and landslides. The community is taught how to reforest forests, so they are free

from floods and landslides. Bare forests cause hot air and flash floods. After several years, the forest became fertile again, filled with shady trees. The air becomes clean, and there are no more floods and landslides.

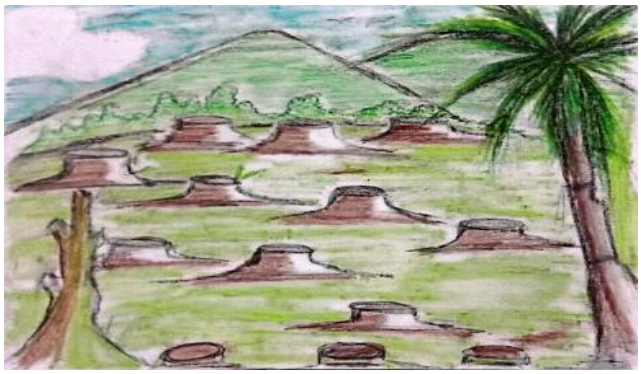

Figure 4. The results of the drawing work of group 1 training participants

3.4.2 Group 2, Title: Waste Causes Floods

Kamishibai's narrative entitled Garbage Causes Floods.

One day, on a sunny morning, a boy named Udin was walking around a river full of rubbish. Then Udin thought, why does this river have so much rubbish? Where does this rubbish come from? Udin was sad to see the river flow blocked because it was full of rubbish. Udin saw Ogal throwing rubbish into the river. Udin saw Ogal throwing rubbish into the river because it was full of rubbish. Udin saw Ogal throwing rubbish into the river. The waste is of various types, including organic and plastic waste. Udin was very surprised to see the rubbish; it turned out that several residents were also throwing rubbish in the river. Over time, the river becomes dirty with rubbish and the river's flow is blocked because the rubbish piles up. After that, over time, the river became polluted and smelly. This polluted river is very damaging to the environment around the river. Finally, to overcome this problem, the village head created a rubbish dump near the village so that people would not throw rubbish into the river because it would cause flooding, damaging the environment. People are apprehensive about the floods that will come when the rain comes. Therefore, people clean up rubbish in rivers, preventing flooding. Once clean, everyone will be happy with a clean river without trash and protected from flooding.

Figure. 5 The results of the drawing work of group 2 training participants

3.4.3 Group 3, Title: Rescue Bell

Village occupation has occupied the volcanic slopes in peace for decades. This is where Deni grew up under the care of his grandparents. Several years later, when he was growing up, the volcano began to emit smoke. This went on continuously for months. Until one day, there was much smoke followed by a thunderous roar. Deni went straight to the kamling post and hit the rescue bell. Hearing clapping, people came out of breath and asked, "What's wrong?" The mountain will erupt, said Deni; “I know where a safe place is, said Deni.

While the residents were getting ready, the village head called the disaster management agency, after which the village head looked for vehicles to evacuate the residents, especially children and the elderly. Thanks to Deni's alertness, all the residents were successfully evacuated and saved.

Figure. 6. The results of the drawing work of group 3 training participants

3. CONCLUSION

Schools are the most effective vehicle for increasing disaster literacy among the community (Juhadi, 2021). More teachers will be able to make learning media with training in making learning media for disaster mitigation. It is hoped that there will be more teachers who can teach disaster mitigation so that more and more people will understand how to deal with disasters, whether earthquakes, landslides, floods, or strong winds.

ACKNOWLEDGMENTS /

I would like to thank the disaster mitigation education training participants who participated in this research activity.

REFERENCES

1. Washington, D.C: National Academies Press; 2011. National Research Council (U.S.). Committee on National Earthquake Resilience – Research Implementation and Outreach. National Research Council (U.S.). Committee on Seismology and Geodynamics. National Research Council (U.S.). Board on Earth Sciences and Resources. National Earthquake Resilience: Research, Implementation, and Outreach.
2. Tuladhar G, Yatabe R, Dahal RK, Bhandary NP. Assessment of disaster risk reduction knowledge of school teachers in Nepal. Int J Health Syst Disaster Manag. 2015;3:20.
3. Collymore J. Disaster management in the Caribbean: Perspectives on institutional capacity reform and development. Environ Hazards. 2011;10:6–22.
4. Muzenda-Mudavanhu C, Manyena B, Collins AE. Disaster risk reduction knowledge among children in Muzarabani district, Zimbabwe. Nat Hazards. 2016;84:911–31.
5. Kagawa F, Selby D. Ready for the storm: Education for disaster risk reduction and climate change adaptation and mitigation1. J Educ Sustain Dev. 2012;6:207–17.
6. Rohrmann B, editor. Risk Perception, Risk Attitude, Risk Communication, Risk Management: A conceptual Appraisal. Conference Presented at the International Society of Emergency Management. 2008
7. Faber MH, Giuliani L, Revez A, Jayasena S, Sparf J, Mendez JM. Interdisciplinary approach to disaster resilience education and research. Procedia Econ Finance. 2014;18:601–9.
8. O'Brien G, O'Keefe P, Rose J, Wisner B. Climate change and disaster management. Disasters. 2006;30:64–80.
9. Hiwaku K, Shaw R. Proactive co-learning: A new paradigm in disaster education. Disaster Prev Manag. 2008;17:183–98.
10. Masuda Z, Yamauchi C. "The Effects of Female Education on Adolescent Pregnancy and Child Health: Evidence from Uganda fs Universal Primary Education for Fully Treated Cohorts," National Graduate Institute for Policy Studies. 2017:01–17.
11. Cummings GE, Corte FD, Cummings GG. Disaster medicine education for physicians: A systematic review. Int J Disasters Med. 2006; 4:36–125.
12. Mir'Atul Azizah, Adi Subiyanto, pengaruh pebahan Iklim Terhadap Bencana Hidrometeorologi di Kecamatan Cisarua-Kabupaten Bogor
13. March 2022PENDIPA Journal of Science Education 6(2)
14. Juhadi, Hamid N, Trihatmoko E, Herlina M, and Aroyandini E N. Developing a Model for Disaster Education to Improve Students' Disaster Mitigation Literacy. Journal of Disaster Research Vol.16 No.8, 2021.

Energy, Environment and Storage

Journal Homepage: www.enenstrg.com

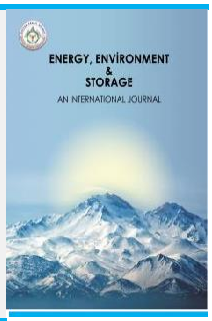

Comparison of Cooling Loads of a Building in the Site with Heat Balance and Radiation Time Series Methods and Computer Aided Analysis

Mehmet Çolak[1], Yasin Kaya [2*], Sebahattin Ünalan[3],

[1]*Erciyes University, Faculty of Engineering, Department of Mechanical Engineering, Kayseri, Turkey*

mehmetcolak58@hotmail.com ORCID*: 0009-0005-2895-5081*

[2]*Erciyes University, Faculty of Engineering, Department of Mechanical Engineering, Kayseri, Turkey*

yasin-3858@hotmail.com ORCID: 0009-0006-6054-2786

[3]*Erciyes University, Faculty of Engineering, Department of Mechanical Engineering, Kayseri, Turkey*

s-unalan@erciyes.edu.tr ORCID: 0000-0002-5605-2614

ABSTRACT. Recently, extensive research has been conducted on energy saving in the buildings. Cooling loads and heat gains stand out as a pivotal factor influencing energy consumption, underscoring the critical need for accurate calculations. This study aims to compare Radiation Time Series and Heat Balance methods, recognized as optimal approaches for cooling load calculations in the ASHRAE Handbook, utilizing computer software. The primary focus of this investigation was a four-floor U-type geometry primary school in Kayseri, comprising 116 space and 93 zones. The building was modeled using Revit software, employing Radiant Time Series method, and IESVE software, incorporating Heat Balance method. All relevant data inputs were defined, and subsequent cooling load calculations were executed. The outcomes reveal with Revit producing a total cooling load estimate 0.6% lower than IESVE. In conclusion, the values derived from both RTS and HB methods for calculating the building's cooling loads exhibit noteworthy proximity, affirming the robustness of these methodologies in conjunction with computer software applications.

Keywords: Cooling Loads, RTS, HB, Revit, IESVE

Article History: Received: 05.01.2024; Accepted: 18.01.2024;

Doi: https://doi.org/10.52924/PODW1839

1. INTRODUCTION

E. Mushtaha et. al. simulated a building with using IESVE, inputing parameters such as shading devices, ventilation and building materials to reduce the cooling load requirement [1]. S. Dagher et. al. analyzed a school building in Minneapolis using IESVE software for energy and daylighting analysis [2]. M. H. Elnabawi investigated the comparison of Revit (Building Information Modeling) with Designbuilder-IESVE (Building Energy Modeling). The problems encountered while importing the project Revit to Designbuilder and IESVE and some improvements suggested that needed to be made working in these software [3]. Kaya Y. modeled U-type building by Revit and researched cooling loads trends for different orientation of building [4]. As can be seen in the studies, it is important to use software that calculates cooling loads such as Revit (Radiant Time Series method) and IESVE (Heat Balance method).

The first and most significant factor for designing an air conditioning system to function accurately throughout the year is to have precise heating and cooling load calculations. This ensures the determination of correct device capacities at the design stage. When calculating heating loads, peak time is equal to coldest ambient temperature time. However, calculating cooling loads is more complex and challenging than calculating heating loads. Because cooling peak time can vary greatly depending on the number of people in the place, devices, lightings and most of all the position of the sun. To address this complexity, it is crucial to choose the most accurate calculation method and leverage computer software support. The cooling load calculation methods in the ASHRAE Handbook, several approaches was found suitable: TETD/TAM (Total Equivalent Temperature Difference Time Averaging Method), CLTD/SCL/CLF (Cooling Load Temperature Difference Solar CoolingLoad-Cooling Load Factor), TFM (Transfer Function Method), RTS (Radiant Time Series) and HB (Heat Balance). HB method, which is called the exact solutionand is the basis of the cooling load calculation methods proposed to date, is complex and requires the use of computers[5].

Software applications like IESVE and Carrier HAP v6 employ HB method, while Revit, using RTS method, can calculate loads [6]. Fig. 1 provides information about the accuracy and complexity of load calculation methods, considering the softwares utilizing these methods [7].

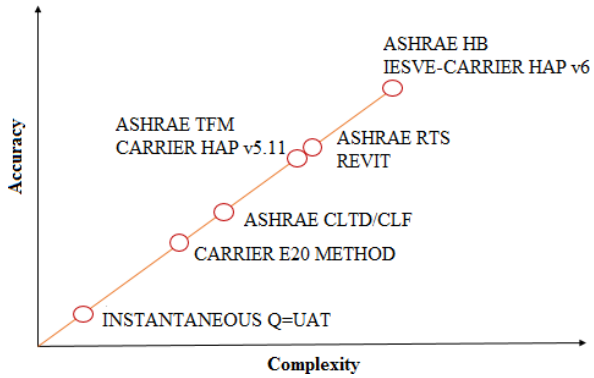

Fig. 1. Accuracy and Complexity for Load Calculations for Different Softwares

In this study, the architectural project of a primary school building in Kayseri was created using Revit. Subsequently, the required designs and data inputs were specified in Revit MEP. Following this, the school building, along with the surrounding high-rise buildings and local shading devices, was modeled using IESVE, with the same data inputs defined in IESVE. Fig. 2 depicts the location and photographs of the school [8].

Fig. 2. Primary School Photographs

2. MATERIALS AND METHODS

2.1 Radiant Time Series Methodology

RTS is a simplified method for calculating cooling load which is derived from HB method. As such, the use of RTS is more important than the use of all other simplified methods (TFM, CLTD/CLF method and TETD/TA method) [5]. The advantages of using this method which is the general procedure for calculating the cooling load of each load component (lights, people, walls, roofs, windows, appliances, etc.) with RTS is as follows:

• A 24-hour profile of component heat gains is calculated for the design day (for conduction; firstly conduction time delay is considered by applying conduction time series).
• Heat gains are splited into two forms, the radiation and convection parts.
• Appropriate radiation time series are applied to the radiation part of the heat gains to account for the time delay in conversion to cooling load.
• The convection portion of the heat gain and the delayed radiative portion of the heat gain are added to determine the cooling load of each component for each hour.

After calculating the cooling loads of each component for each hour, these components are summed to determine the total cooling load and the hour of peak load is determined for the design of the air conditioning system. This process is repeated over multiple design months to determine the month in which the highest load occurs [6]. Fig. 3 illustrates RTS methodology.

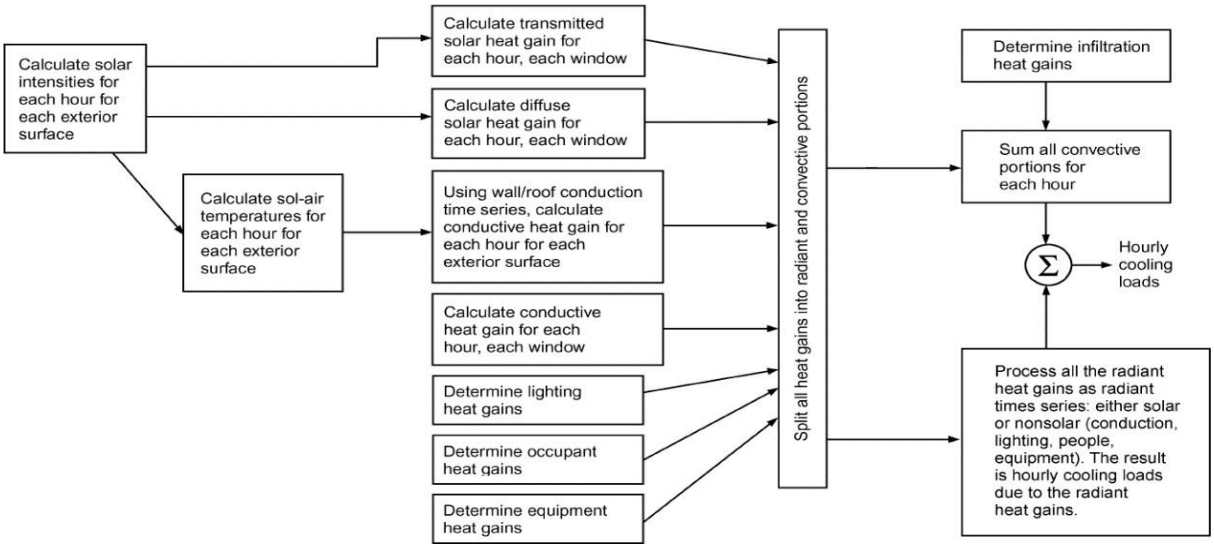

Fig. 3. Radiant Time Series Methodology

2.2 Modeling by Revit

Shapes, structures and systems in 3D and generated plans, elevations, schedules, sections, and sheets can be modelled by Revit. Afterwards, Building Information Modeling (BIM) can be created and modeled for the purpose of designing mechanical or electrical system design. Cooling and heating loads can be calculated in a BIM process. Revit uses RTS method for these calculations. And also, Revit can analyze the energy performance of buildings [9].

3D photographs and floor plans of the school modeling by Revit are shown in Fig. 4, 5, 6, 7, 8. Within the building, there are indoor areas with many different functions such as classroom, library, gym, school canteen, corridor, office enclosed, infirmary, storage, restrooms. 116 spaces and 96 zones were created according to the areas of use in the building. Input datas defined for the characteristics of these spaces and zones. The same process was done on IESVE.

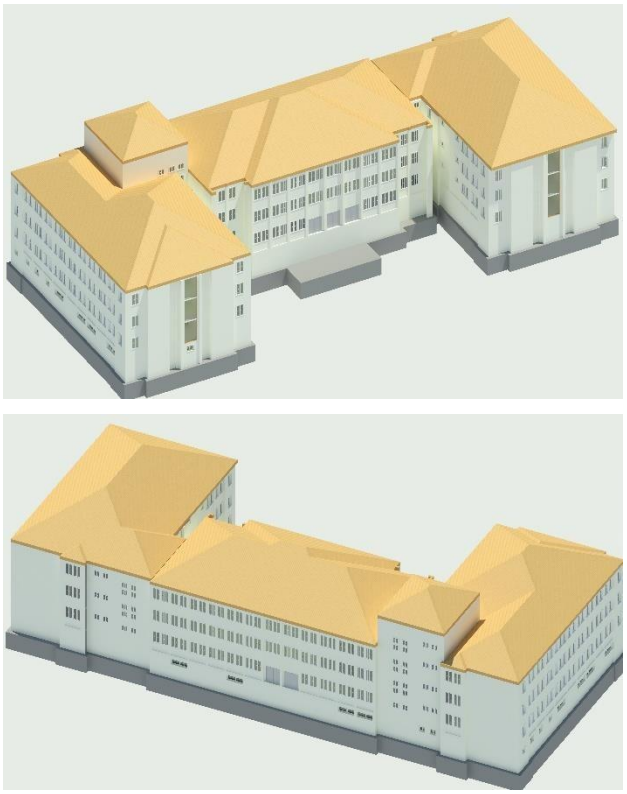

Fig. 4. Primary School 3D Photographs on Revit

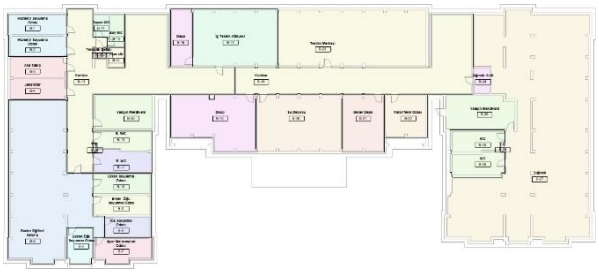

Fig. 5. Basement Floor

Fig. 6. Ground Floor

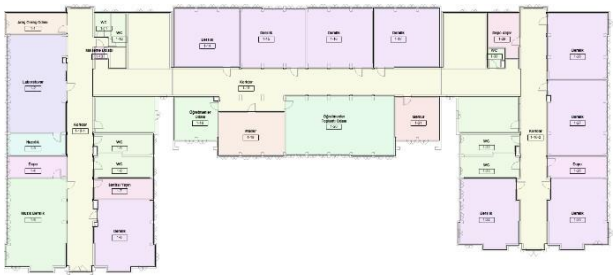

Fig. 7. First Floor

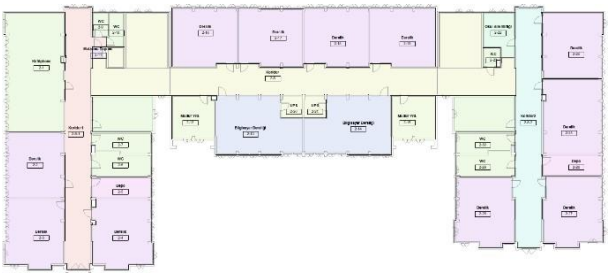

Fig. 8. Second Floor

2.3 Heat Balance Methodology

Cooling load determination involves calculating a surface-to surface conduction, convection, and radiative heat balance for each room surface and a convection heat balance for the room air. The HB method, which forms the basis of cooling load calculations, solves the problem directly rather than applying conversion based procedures. The advantages of this method is containing no arbitrarily set parameters and does not eliminate any operations [5].

The HB Method calculates time delay effects explicitly with some basic assumptions like uniform surface temperatures. Conductive, convective, and radiative heat balance are calculated directly for each surface within a room [10]. Heat Balance method has four distinct processes:

- Outdoor face heat balance
- Wall conduction process
- Indoor face heat balance
- Air heat balance

A process detailed in the accompanying Fig. 9 clearly illustrate the relationships for a sample opaque surface. The processes duplicated for each surface covering the whole zone. Similarly, this can be applied for transperant surfaces. However, absorbed solar energy by the building components conducts the heat inside and a portion of solar incident is not reflected back to the sky and transmitted to inside. These heat gain or losses affect the surface heat balances. [5].

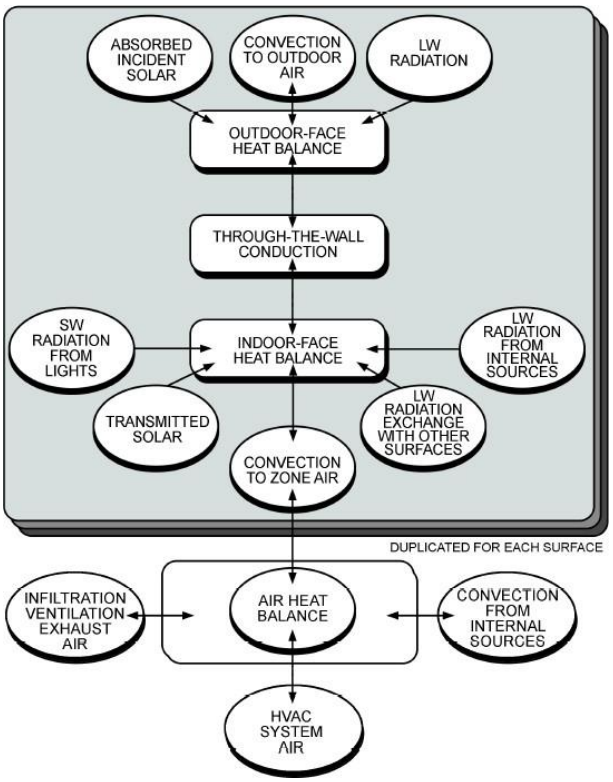

Fig. 9. Heat Balance Methodology

The ASHRAE Heat Balance Method states that the "sum of all space instantaneous heat gains at any given time does not necessarily (or even frequently) equal the cooling load for the space at that same time". Fig. 10 attempts to convey this phenomenon by demonstrating the time delay associated with the 'Gains vs Loads' discussion [6].

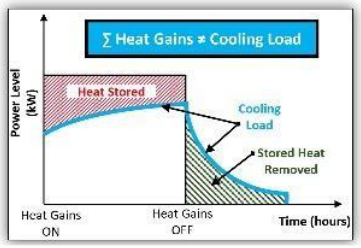

Fig. 10. Thermal Storage Effect in Cooling Load From Internal Gains

2.4 Modeling by IESVE

IESVE is a Building Energy Modeling (BEM) Software that perform calculations for industry standard heating and cooling loads including options for the ASHRAE Heat Balance method or CIBSE Admittance method with IESVE. IESVE assesses daylight metrics for LEED & BREEAM such as Spatial Daylight Autonomy (sDA) and Useful Daylight Illuminance (UDI). It performs minimum ventilation calculations, evaluates outdoor air supply from mechanical HVAC systems or natural ventilation design. Furthermore, it uses Computational Fluid Dynamics (CFD) airflow simulation to evaluate occupant comfort and overheating potential. In addition to this it can evaluate predictive metrics for site energy, source energy, energy cost and carbon emissions by using the world-renowned APACHE simulation engine [11].

3D photographs and floor plans of the school modeling by IESVE are shown in Fig. 11, 12, 13, 14, 15. The drawings

that appear green colors show the shading elements that cause local shading, and the drawings that appear pink colors show the shading of adjacent buildings. Since the shading effect cannot be calculated with drawing on Revit, the shading effect was not included in the calculations on IESVE for comparation of methods.

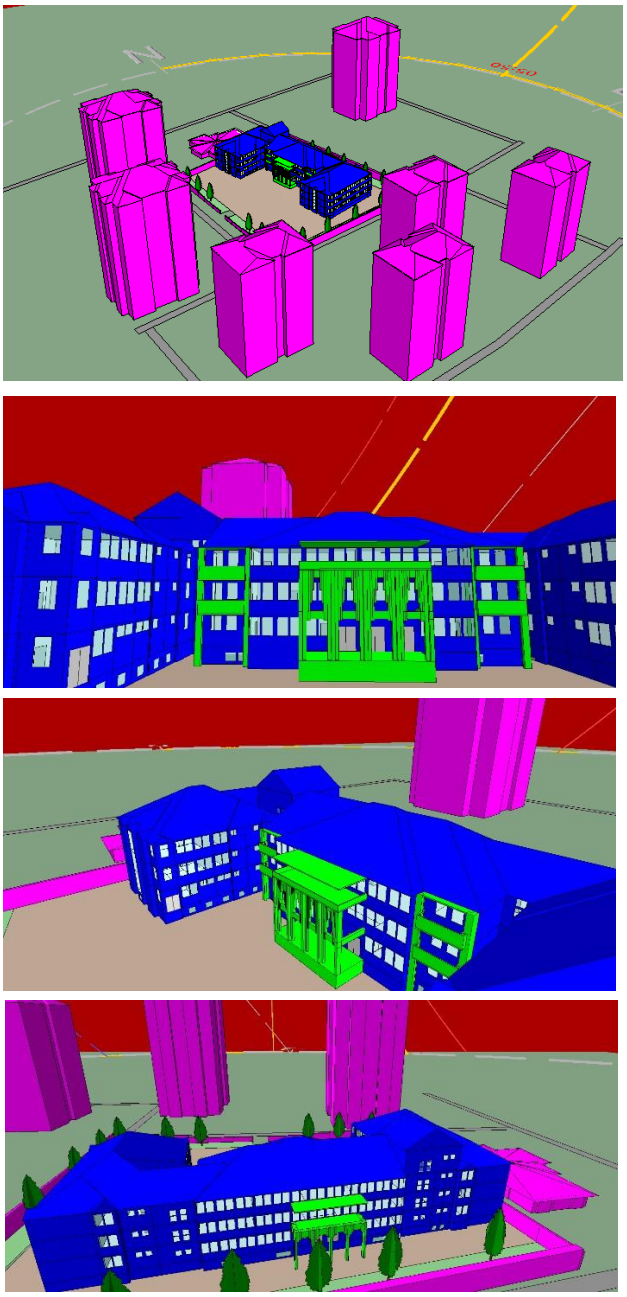

Fig. 11. Primary School 3D Photographs on IESVE

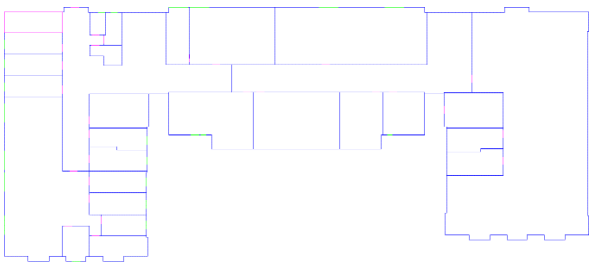

Fig. 12. Basement Floor

Fig. 13. Ground Floor

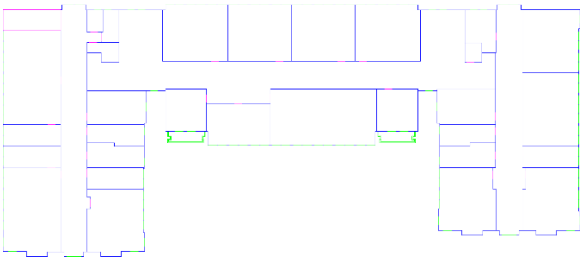

Fig. 14. First Floor

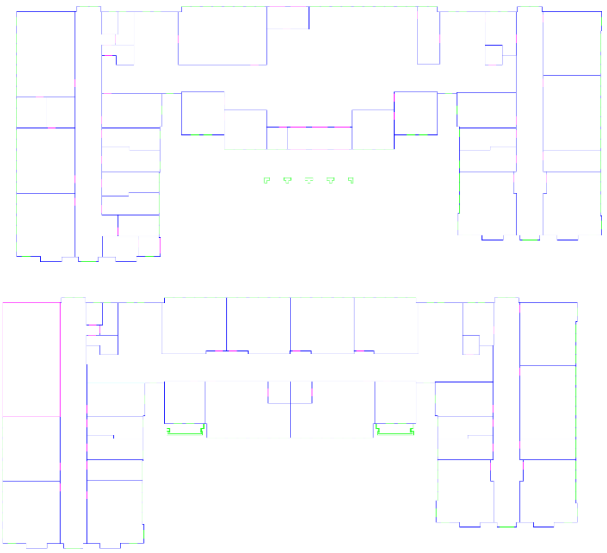

Fig. 15. Second Floor

2.5 Data Inputs

Accuracy of calculations and results is of great importance comparing two calculation methods. For this reason, separate modeled were created for both software. Revit's drawing technique, wall thicknesses can drawn, but IESVE, only line drawings can drawn. This causes small deviations in internal areas. However, because heat gains are low on the wall, this is negligible. Many data inputs need to be defined on both Revit and IESVE. In order to compare 2 software and 2 different calculation methods, all data inputs defined same in softwares which were shown Tables 1 and 2. Kayseri city chose for design weather data on Revit and IESVE.

Table 1 Parameters and Data Inputs

Parameters	Data Inputs
Space Types	Classroom-Library-Gym-School Canteen-Corridor-Office Enclosed Infirmary-Storage-Restrooms
Number of People	Numbers specific to each space were entered
Lighting and Power Loads	Space specific option selected and these values entered.
Occupable Schedules	8 AM to 6 PM
Lighting Schedules	4 PM to 6 PM
Cooling Set Point	23 °C
Cooling Air Temperature	12 °C

Table 2 Construction Types

Construction	U (Overall Heat Transfer Coefficient W/m².K)	SHGC (Solar Heat Gain Coefficient)
Exterior Walls	0,8108	
Interior Walls	1,4773	
Floors	1,361	
Slabs	0,7059	
Doors	3,7021	
Exterior Windows	1,9873	0,39
Roof	0,6819	

3. RESULTS AND FIGURES

Through the analysis, it was ascertained that Revit and IESVE produced total cooling load estimates of 411.11 kW and 413.64 kW, respectively, resulting in a discrepancy of merely 0.6%. A detailed breakdown of the cooling loads for individual floors, as assessed by both Revit and IESVE, is illustrated in Fig. 16. A visual examination of these graphics reveals a noteworthy consistency, with cooling load values in nearly all zones exhibiting close proximity to each other.

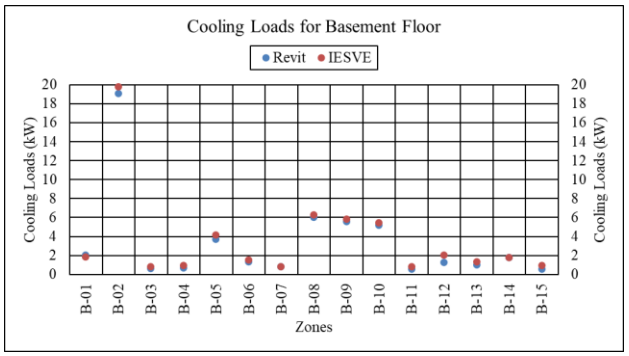

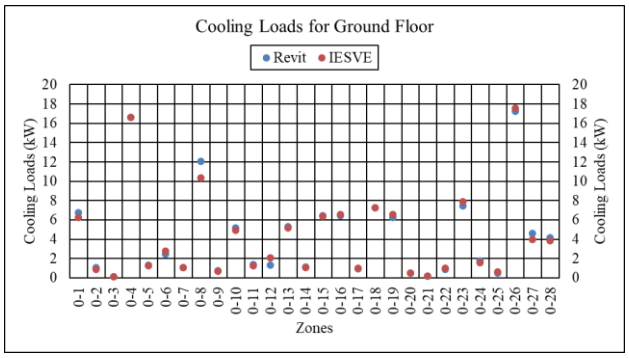

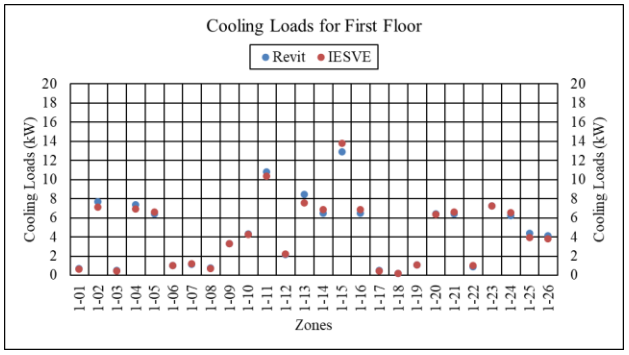

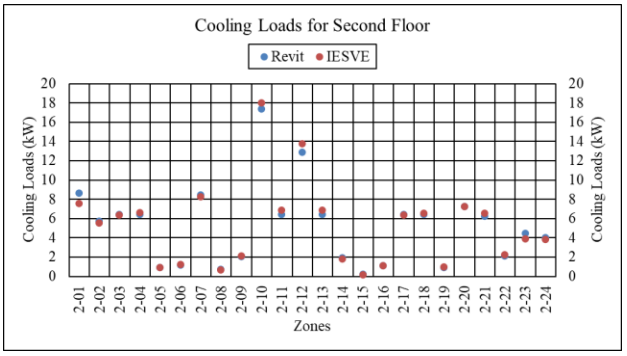

Fig. 16. Comparison of Cooling Loads of Each Floor by both Revit and IESVE

When calculating the cooling loads by Revit, if the building is exposed to shading, it cannot calculated the effect of shading on the cooling load. On the contrary, cooling loads with and without the shading effect were calculated by IESVE. In addition, it is not possible to select the calculation date range when cooling loads are calculated by Revit, but date range can be selected on IESVE. In other words, if desired, the results can be further optimized by selecting date ranges which cooling loads are important.

In this study, RTS and HB methods were compared by Revit and IESVE and shading effect neglected. Apart from this study, both shading effect and June-August date range selected on IESVE and building was simulated again. As a result of the calculations, the total cooling load was 389.8 kW. In other words, self-shading, local shading, and shading of adjacent buildings reduced the total cooling load of the building by 5.8%.

4. CONCLUSION

In previous studies with by using Revit and RTS:

Laxi et. al. were calculated cooling loads of a hotel building by two methods, RTS method by Revit and CLTD/CLF/SCL method, compared cooling loads are closely approximate each other by acceptable range of 10% [12]. Matej modeled a referential building, calculated cooling loads with Revit and then compared Revit to Energie 2015 software in terms of energy performans [13]. Nabin was created a residential building by Revit and calculated heating and cooling loads with RTS method [14]. Vittoria et. al. was modeled The Maritime Station of Naples by Revit and DesignBuilder softwares to compare cooling loads. Cooling peak loads was calculated 3,333 ve 3,055 kW respectively [15].

In previous studies with by using IESVE and HB:

Zohaib et. al. were generated Dynamic Thermal Simulation by IESVE which models residential spaces. The energy consumption reduced by 8% and cooling loads by 20% by using Variable Speed Drive instead of using fan coil [16]. Baskara et. al. studied Geometrical model which is a student dormitory. Seven stories was created by IESVE. Heat gains were comperad to ventilation, solar, lighting, people, equipment. They figured out that the most heat gain parameter was ligthting [17]. Sigalingging et. al. were modeled the building (6mx10mx2.85) plan and then it has been simulated by IESVE with the Passivhaus standard. It was calculated 11.41 MWh for original layout, 10.89 MWh for the house with Passivhaus application in terms of annual

cooling energy use [18]. Budiyanto et. al. were selected a refrigerated container for estimated of energy consumption based on the cooling loads. Research was conducted in two stage, firstly the measurement data were obtained from the experimentation, later container was modeled by IESVE. Energy consumption was compared with IESVE result and measurement data. Both study results were found to be compatible with each other [19].

Numerous methodologies and software applications are employed for the computation of cooling loads, with RTS and HB methods recognized as the most precise albeit intricate. Within the scope of this investigation, a comparative analysis was undertaken between the RTS and HB methods, revealing no substantial disparities in the resulting calculations.

Regarding the software employed, Revit stands out for its capacity to generate detailed architectural projects. Its notable feature lies in employing the RTS method for the calculation of cooling loads. However, it is worth noting that Revit lacks the capability to factor in the effects of shading on cooling loads within its drawings. Conversely, IESVE serves as a thermal analysis calculation software, offering the distinct advantage of calculating shading effects on cooling loads, coupled with its utilization of the HB method.

REFERENCES

[1] E. Mushtaha, T.Salameh, S. Kharrufa, T. Mori, A. Aldawoud, R. Hamad ve T. Nemer, The impact of passive design strategies on cooling loads of buildings in temperate climate, 2021, Case Studies in Thermal Engineering, Volume 28.

[2] S. Dagher, B. Akhozheya ve H. Slimani, Energy analysis studying the effect of solar shading on daylight factors and cooling hours in an extreme weather, 2022, Energy Reports, Volume 8: 443-448.

[3] M. H. Elnabawi, Building information modeling-based building energy modeling: Investigation of interoperability and simulation results, 2020, Frontiers in Built Environment, Volume 6.

[4] Kaya Y., 2020. Numerical investigation of the effect of buildings location plans on the cooling load, Erciyes University, Master Thesis, Kayseri.

[5] Ashrae Handbook Committee, 2021. Nonresidential cooling and heating load calculations, pp. 18.17-18.25, ASHRAE Handbook-Fundamentals, Atlanta.

[6] Web pages: https://www.iesve.com/discoveries/article/10017/ashrae-heating-and-cooling-load-calculations https://www.carrier.com/carrier/en/worldwide/news/news-article/carrier-releases-hap-v6--a-major-upgrade-to-hvac-system-design-software.html https://help.autodesk.com/view/RVT/2020/ENU/?guid=GUID-D88E8A06-6E08-4CD6-89A0-368A2AD6C03C (Dated access: January 2024).

[7] Yıldız A., Ersöz M.A., Altıner A., Bilki T.B., Computer aided analysis of cooling load calculations, 12th national plumbing engineering congress, İzmir, 2015, MMO.

[8] Web page: https://parselsorgu.tkgm.gov.tr/#ara/cografi/38.789566937045954/35.61383485794068 (Dated access: January 2024).

[9] Web page: https://www.autodesk.com/solutions/revit-vs-autocad (Dated access: January 2024).

[10] Web page: https://www.iesve.com/discoveries/blog/3348/ashrae-heat-balance-method-radiant-time-series-whats-the-difference (Dated access: January 2024).

[11] Web page: https://www.iesve.com/software/virtual-environment (Dated access: January 2024).

[12] Laxmi G., R L. S., Bim-Based energy performance modeling and simulation of hotel building, 2023, Journal of Data Acquisition and Processing, Volume 38: 237-255.

[13] B. Matej K., 2018. Implementation of BIM systems for energy analysis and optimization in buildings, Czech Technical University In Prague, Master Thesis, Prague.

[14] Nabin T., 2020. Enhancement of HVAC load, energy consumption and energy cost for a proposed residential building, Thesis, Nepal.

[15] Vittoria B., Alberto C., Alessandro M., Gennaro N., On the interoperability of building information modeling for energy analysis: the case study of the Maritime Station of Napoli (Italy), IOP Conference Series: Earth and Environmental Science, 2022.

[16] Zohaib S. , Hassam N. C., Energy modelling and indoor air quality analysis of cooling systems for buildings in hot climates, 2018, Fluids.

[17] S. A. Baskara, G. S. Adi, S. S. Utami, B. Prayitno, and FX P. J. Guntoro, Cooling load analysis in asrama kinanti 1 ugm using building performance simulation, 2020, IOP Conference Series: Earth and Environmental Science, Volume 520, Indonesia.

[18] R. C. Sigalingging, D. Chow and S. Sharples, Modelling the impact of ground temperature and ground insulation on cooling energy use in a tropical house constructed to the Passivhaus Standard, 2019, IOP Conference Series: Earth and Environmental Science, Volume 329, Cardiff, Wales.

[19] M. A. Budiyanto, Nasruddin, F. Zhafari, Simulation study using building-design energy analysis to estimate energy consumption of refrigerated container, 2019, Energy Procedia, Energy Procedia, Volume 156: 207-211.